Elucidation of Core-shell Structure in Phenyl Grafted Carbon Nitride/TiO_2 Nanohybrids for Visible-light Mediated H_2 Production with Simultaneous Rhodamine B Degradation

Moulika Hazra [a], Stefania Porcu [a], Stephen Nagaraju. Myakala [b], Hannah Rabl [b], Dominik Eder [b], Alexey Cherevan [b], Pier Carlo Ricci [a]**

[a] Department of Physics, University of Cagliari, Complesso Universitario di Monserrato S.P. Monserrato-Sestu Km 0,700 09042 Monserrato (CA) – Italy

[b] TU Wien, Institute of Materials Chemistry, Division Molecular Materials Chemistry, Getreidemarkt 9/BC/02, 1060, Vienna, Austria

* Corresponding authors

E-mails: moulika.hazra@unica.it, stefania.porcu@dsf.unica.it, stephen.myakala@tuwien.ac.at, hannah.rabl@tuwien.ac.at, dominik.eder@tuwien.ac.at, alexey.cherevan@tuwien.ac.at, carlo.ricci@dsf.unica.it

ABSTRACT: Dual-function photocatalysts help to maximize resource utilization in water remediation but often they are visible light inactive, toxic and cost-intensive. Herein, a Type II heterojunction visible light active photocatalyst is reported for a tandem degradation of Rhodamine B and generation of H_2. A Rhodamine B degradation rate of $2.3x10^{-2}$ min^{-1} and H_2 production activity of 5789 μmol $h^{-1}g^{-1}$ is shown. The hybrid shows gradient core-shell morphology with a visible light absorbing phenyl-modified carbon nitride (PhCN) core and a porous PhCN-TiO_2 outer shell, resulting in enhanced interaction between the catalyst and the surroundings. The nanoscale crystallization of TiO_2 on PhCN's surface shifts the triazine network structure, while autoclave treatments further increase the band gap and suppress charge carrier recombination. The influence of nanoscale morphological changes on photocatalytic activity was examined by varying the component ratios and thermal treatments, highlighting the strong correlation between nanoscale architecture and enhanced catalytic activity. This work provides a detailed guide on the exploration of environmentally friendly dual-functional photocatalysts.

KEYWORDS: Dual-Function Photocatalysis, Core-Shell, Visible-Light Photocatalysis, H_2 Production, Type II Heterojunction, PhCN/TiO_2 Hybrid

Abbreviations: PhCN= Phenyl-modified Carbon nitride, DFP= Dual-functional Photocatalysis, RT= Room Temperature, STE= Self-Trapped Excitons, TRPL= Time-Resolved Photoluminescence, rad= radiative, NR= Non-Radiative, tot= Total, RhB= Rhodamine B, TEOA= TriEthanOlAmine, MeOH= Methanol

1. INTRODUCTION

Rapid industrialization has resulted in the pollution of natural water bodies which has led to disruption of the local flora and fauna along with disruption in climate regulation via stormwater runoff, erosion, and harmful algal blooms. According to the United Nations World Water Development report 2024, due to the global scarcity of water, 3.5 billion people lack the access to clean water resources.[1] With growing energy demands across the globe, increasing prevalence of water-borne diseases and declining freshwater resources stringent measures for treatment of industrial wastewater have become of high importance for regional governmental policies to avoid conflicts on water resources.[1] It has become obligatory to develop advanced, environmental friendly, low-cost, and high-efficiency reclamation of wastewater.

Dual-functional photocatalysis (DFP) appears as a suitable technique with the potential to be applied for synergistic degradation of industrial pollutants in the wastewater. This is an upgrade to the traditional photocatalysis[1] process where a photocatalyst can be utilised to degrade pollutants present in the water via photocatalytic oxidation and simultaneously generate the clean fuel (e.g. H_2 gas) via proton reduction by the consumption of light energy. This dual-function approach utilises both photogenerated electron and holes in a photocatalyst to their full potential and aligns with circular economy principles, where waste products (pollutants) are converted into valuable resources (solar fuels).

In recent years, various works have reported novel DFP materials ranging from metal-organic frameworks[2,3,4], metal-sulphide based composites[5 ,6] and TiO_2 based hybrids[7,8] all the way to graphitic carbon nitride (gCN) based materials[8,9], etc. Although the visible-light activity of the gCN based hybrids make them promising candidates for practical utilisation, it suffers from high rates of electron-hole recombination, which significantly reduces its photocatalytic efficiency.[10] Thus, methods like doping[10], precursor pre-treatment[11], surface modification[9] and copolymerisation[12] have been employed to improve its photocatalytic efficiency. The studies on DFP systems using gCN face challenges to utilise the solar-light efficiently due to low visible-light activity or report complex methods of material synthesis incorporating expensive precursors and non-biofriendly materials which are not ideal for commercialization of the end-product.[13] Lately, phenyl-based modifications of gCN have been reported to enhance the charge carrier migration and separation, and lower the bandgap of gCN.[12,14–16] The incorporation of phenyl groups improves the light absorption of gCN by tuning its band structure and facilitates the separation of photogenerated carriers by accelerating the electron transfer from the tri-s-triazine rings to the introduced aromatic rings.[12,14,16] When hybridised with anatase phase of TiO_2, phenyl-modified carbon nitride could provide exceptional visible-light sensitising to the chemically stable, highly active and naturally abundant and bio-friendly TiO_2 anatase. The reported works on gCN/TiO_2 hybrids used in phenolic degradation[17], organic dye removal[18], antibiotic degradation[19,10], photo-electrocatalytic processes[20], oxygen reduction reaction (ORR)[21], viral disinfection[22], hydrogen evolution reaction (HER)[9] , etc indicate possible successful research on PhCN/TiO_2 hybrids for DFP applications. Special emphasis has been placed on core-shell structured photocatalytic systems in recent times for their high activity as compared to other morphologies[20,21,23] demonstrating the importance of morphology in a hybrid photocatalytic system. The core-shell architecture has shown enhanced charge transfer abilities with efficient use of the material due to high surface to volume ratio which lowers the cost of material production.[24] Several works have reported a TiO_2 core and gCN shell for enhanced photocatalysis[19,23,25,26], but this architecture prevents the interaction of the active sites on the TiO_2 surfaces with the surrounding pollutant molecule in addition to the shielding of

gCN core by the shell leading to low visible-light absorption. Wei et al demonstrated the importance of mesoporous structures, allowing higher interactions with the reaction molecules in photocatalysis which could address the challenges of these gCN/TiO_2 systems.[17]

Hence, we aimed to develop a hybrid system with PhCN core and TiO_2 shell with a greater intermeshed network of the two components. The nanoscale architecture of the hybrid would guarantee a high charge carrier migration from the sensitiser to TiO_2 surface leading to a high photocatalytic activity. The photocatalytic prowess of such a hybrid system is significantly dependent on its structural, chemical and optoelectronic properties, which are not necessarily identical to the individual properties of the constituent materials[27] and strongly depend upon the synthesis conditions[28]. For instance, particle size determines the amount of available surface area and catalytic active sites[29]. The Chen and Wunderlich model modified Avrami equation provides certain guidance here as it establishes that high precursor dosage can resist nucleation, decrease the nucleation number, and increase the particle size.[30] In another relevant work, Brinker and Scherer reported the decrease in the catalytic performance of larger particles formed due to the agglomeration of smaller particles with high surface energy.[31] Therefore, all these properties of a material are intertwined with each other and are not exclusively responsible for the photocatalytic activity. Hence, designing a perfect photocatalyst is a challenging task which requires an in-depth understanding of the structural, chemical and optoelectronic properties of the material which can then be used to tune them via different synthesis techniques and treatment procedures.

In this work, we elaborate the streamlining procedure of a hybrid photocatalyst consisting of phenyl-modified carbon-nitride (PhCN) and anatase TiO_2 with a greater emphasis on evolution of the structural and optoelectronic properties of the constituents as well as their complex interplay towards its photocatalytic behaviour. We hypothesise that the growth of TiO_2 on the surface of PhCN leads to alteration in the chemical structure of the later whose extent is dependent on the degree of crystallization of TiO_2 which in turn also affects the properties of the hybrid material and can be controlled by thermal treatment. We found that a high-pressure treatment of PhCN induces possible surface changes which in turn, alter the structural and optical properties of PhCN. The study emphasizes nanoscale engineering, featuring a gradient core-shell structure. A series of hybrids varying the mass ratio PhCN:TiO_2 were synthesized using a solvothermal approach. The interactions between PhCN and TiO_2 with varying mass ratios were thoroughly examined using a variety of characterization techniques. Additionally, the impact of annealing at different temperatures on these interactions was also systematically investigated. The thermal treatment post-hydrothermal process revealed that while it increased the crystallinity and reduced defects in the TiO_2 shell, it also led to a thicker shell. This increased thickness led to reduced charge mobility and consequently, the compounds subjected to thermal treatment at higher temperatures exhibited decreased photocatalytic efficiency. A “gradient core-shell structure” was observed in the hybrids via energy dispersive spectroscopy (EDS), transmission electron microscopy (TEM) and X-ray photoelectron spectroscopy (XPS). The evolution of this core-shell structure with varying Ti precursor mass is illustrated in Figure 1. The impact of nanoscale structural changes on photocatalytic performance was investigated emphasizing the close relationship between nanoscale design and improved catalytic efficiency. The extensive dye degradation tests with rhodamine B (RhB) along with hydrogen evolution reaction (HER) tests suggest the advantageous nature of the gradient core-shell structure by maximising the interaction of the photocatalytic sites with pollutant molecules. Based on the combined results from 3D fluorescence mapping, time-resolved photoluminescence study, and UV-Vis absorption spectroscopy, we report a successful band-gap engineered PhCN/TiO_2 hybrid with excellent visible-light activity for hydrogen gas generation as well as Rhodamine B degradation. These results prove that the formation of higher

number of heterojunctions and increased interaction between the photocatalyst and the pollutant molecules is of utmost importance for the optimum photocatalytic activity. Finally, a type II-scheme heterojunction type charge -transfer mechanism is proposed for the improved PhCN/TiO_2 hybrid for the simultaneous degradation of Rhodamine B dye and H_2 production. To the best of our knowledge, this work is the first to employ phenyl-modified carbon nitride-based hybrid photocatalyst for dual-functional photocatalysis application and underscores the importance of nanoscale feature tuning in developing commercially

viable, high-performance photocatalysts and provides a pathway for future research into DFP systems.

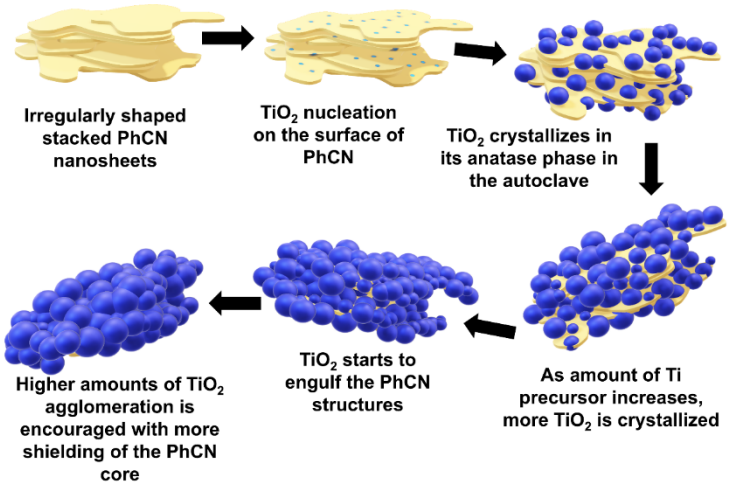

Figure 1 Schematic diagram of the structural evolution of the PhCN/TiO_2 hybrids.

2. EXPERIMENTAL SECTION

2.1. Synthesis of PhCN/TiO_2 hybrid series

A series of PhCN/TiO_2 hybrids were prepared by a facile solvothermal treatment using pristine PhCN and $TiCl_4$*(Supporting information section 1)*. Pristine hybrids were prepared by increasing the amount of $TiCl_4$, denoted as A_RT, B_RT, C_RT and D_RT in the order of increasing Ti content, where RT stands for room temperature denoting the non-annealed samples. Subsequently, each of these hybrids containing different ratios of PhCN:TiO_2 were further annealed at 230˚C, 300˚C and 400˚C, denoted as A_230, A_300, A_400; B_230, B_300, B_400 and so on. Reference samples were also prepared as mentioned in Supporting information.

2.2. Photocatalytic Evaluation

The PhCN/TiO_2 hybrids were evaluated for their photocatalytic performance for Rhodamine B degradation and H_2 production using white light LED bulb and 445nm monochromatic LED source respectively. The Rhodamine B degradation tests were carried out under oxygenated environment while the HER test was carried out under inert conditions. The DFP measurements were done in identical environment to that of HER tests *(See details in Supporting information section 1).* The synthesized hybrids and the reference materials were structurally and optically characterized using instrumentation supplemented in the Supplementary Material.

3. RESULTS AND DISCUSSION

3.1. Structure and Morphology characterization

The phase compositions of the hybrids were studied through powder X-ray diffraction (XRD) (Figure 2a, 2b).

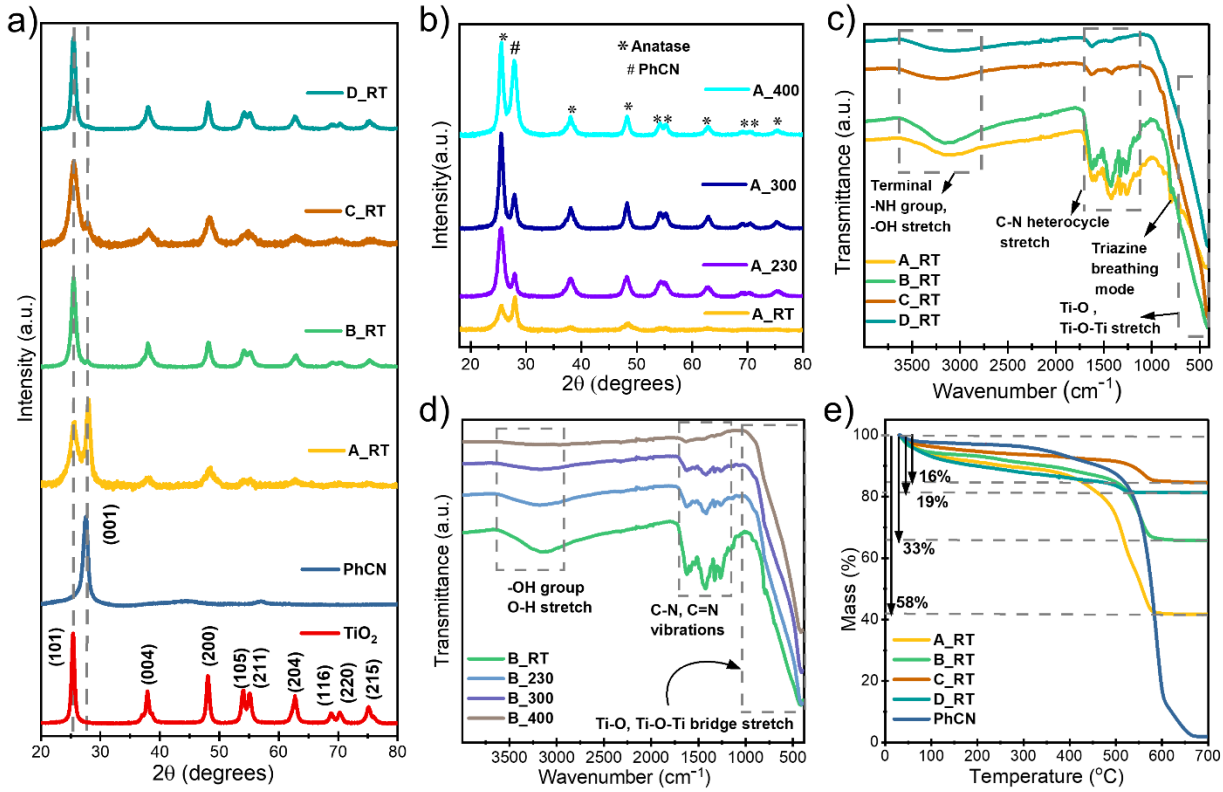

Figure 2. a) XRD of all as-prepared hybrids, pristine PhCN and TiO_2 anatase; b) XRD of the hybrid series A annealed at different temperatures; c) ATR-FTIR spectra of as-prepared hybrids with varying PhCN:TiO_2 ratio; d) ATR-FTIR of hybrid series B annealed at different temperatures; e) TGA graphs for all as-prepared hybrids compared with Bulk PhCN.

The characteristic reflection of PhCN at 27.5˚ corresponding to (001) depicts the interplanar stacking of the system.[16] All the as-prepared hybrids show the presence of titania in its anatase phase, without any contribution of brookite or rutile phases,[10] which can be attributed to the hydrolysis conditions of $TiCl_4$ in a high pH environment at 180˚C known to promote anatase growth.[32] The diffraction from PhCN dies down with increasing TiO_2 content in the hybrids due to the lowering concentration of the PhCN component.[25] The hybrids with lower TiO_2 content also show the PhCN characteristic peak at ~27.9˚ shifted from its original angle in pristine PhCN (Figure 2a). This shift towards higher 2θ can be a result of decrease in the interplanar spacings of its nanosheets because of high pressure treatment in the autoclave. The same effect was observed when PhCN was treated at the same temperature, pressure, and duration in an autoclave as the hybrids without the Ti precursor *(Figure S1).* The XRD peaks of TiO_2 in the hybrids also exhibit a minor shift towards higher 2θ when compared to the characteristic peaks of the pristine anatase. This shift in the crystallographic planes of TiO_2 can be attributed to its interaction with PhCN structure.[10] In comparison to this, no further shifts are observed between

the samples containing different ratios of PhCN:TiO_2, nor after annealing at different temperatures (Figure 2b). The average crystallite sizes calculated using the Scherrer equation ranges from 5 -14 nm for the hybrids *(Figure S2).* It is observed that the crystallite size always grows with annealing temperature for all the hybrids. According to the degree of crystallization calculated by the XRD data *(Figure S3)*, we see an increase in the crystallinity of the hybrid from A_RT to B_RT and similar values for hybrids B_RT, C_RT and D_RT. This could imply that the TiO_2 has the highest degree of crystallization for the hybrid B ratio because hybrid C and D do not show appropriate increase in the % crystallinity in the hybrid system even after possessing a significantly high amount of Ti precursor during the solvothermal treatment. Since the synthesis conditions were the same for all the hybrids, it can be said that the TiO_2 did not find enough solvent molecules for immediate hydrolysis which slowed the process and the total time for the reaction was not enough for the crystallization of Ti species.[33]

The chemical composition of the PhCN/TiO_2 hybrids was studied by attenuated total reflection IR absorption spectroscopy (ATR-FTIR) (Figure2c, 2d). Pristine PhCN shows the characteristic peaks of sp^3 C-N vibrations at 1383, 1324 and 1250 cm^{-1}, and sp^2 C=N vibrations at 1611 and 1534 cm^{-1}, well in agreement with reported literature *(Figure S4).*[34] The band at 810 cm^{-1} shows the breathing mode for triazine units in PhCN[34] – confirming its incorporation – whereas the broad peak in the range of 3500-3000 cm^{-1} corresponds to the terminal N-H groups and adsorbed water molecules in PhCN.[14] Figure 2c shows the successful formation of TiO_2 in the hybrids visible from the appearance of a broad absorption in the low-wavenumber region at 483 cm^{-1}, corresponding to the Ti-O vibration.[34] All hybrids show a broad band between 3500 and 2800 cm^{-1} corresponding to the terminal N-H groups of the PhCN with a decrease in intensity with increasing TiO_2 loading. Moreover, the band 1300-1200cm^{-1} corresponding to an aromatic amine gets weaker alongside other aromatic bond vibrations in samples containing higher titania content, showing a loss in the PhCN structure. When annealed, the hybrids show less surface adsorbed water molecules, lower contribution of sp^3 C-N and sp^2 C=N vibrations along with a stronger Ti-O stretching related to the higher degree of crystallization of the anatase phase and high amounts of TiO_2 (Figure 2d). Complementarily, the RAMAN spectra of the hybrids *(Figure S5)* show the presence of characteristic E_g mode vibration of anatase TiO_2 and the grain development with annealing.

Next, the thermal stability of the pristine components and the hybrids was studied via thermo-gravimetric analysis (TGA) by heating them from room temperature until 700˚C in synthetic air (Figure 2e). PhCN shows a sharp mass loss starting from 500˚C and losing 100% of its mass via thermal oxidation until 650°C, while pure TiO_2 shows no change in mass in this temperature range.[35] The autoclave treatment of PhCN barely alters the nature of the TGA curve *(Figure S7a).* In the as-prepared hybrids, a similar mass drop is observed in the same temperature range, attributed to the PhCN decomposition, and was used to calculate the fraction of PhCN present in these hybrids *(Table S1).* Interestingly, the amount of PhCN in the as-prepared hybrids calculated by the TGA results are lower than the amounts expected from the synthesis conditions. This result indicates a possible loss in the pristine form of PhCN during the hybrid formation via solvothermal treatment. On the other hand, TGA curve of hybrid sample annealed at 400°C (*Figure S7b*) show much lower mass loss due to the presence of highly crystalline TiO_2.

XPS was employed to elucidate the surface composition and nature of the chemical bonds present in the hybrids. In PhCN C1s spectra *(Figure S8)* the chemical bonds N=C-N, C-NH_x and C=C are observed at 288.7 eV, 286.02V and 284.6V respectively.[14] The N1s spectra of PhCN (Figure 3c) shows characteristic peaks of C–N=C, N–(C)3, C-NH, and pi-excitation, at 398.15, 399.43, 401.23, and 404.51 eV respectively.[16] The XPS indicates a successful phenyl-modification of carbon

nitride according to previous reports.[34] The survey spectra of hybrids A_RT, B_RT, C_RT and D_RT show the presence of species from both - PhCN and TiO_2 (Figure 3a). With increasing titania loading in the hybrid, the Ti peaks strengthen and the N1s peak weakens. The calculated atomic % of N depreciates with increased titania loading in the samples and an increase in Ti% is also observed *(Table S2)*. We observe a shift of 0.7 eV in the N1s edge of the hybrids towards lower binding energies as compared to PhCN (Figure 3c) indicating the presence of a more electropositive atom which we attribute to the Ti-neighbour in the hybrids.[23] Furthermore, we also see an increasing contribution from the C-N=C signal and a decreasing contribution from the N-$(C)_3$ component with the increase in TiO_2 content.

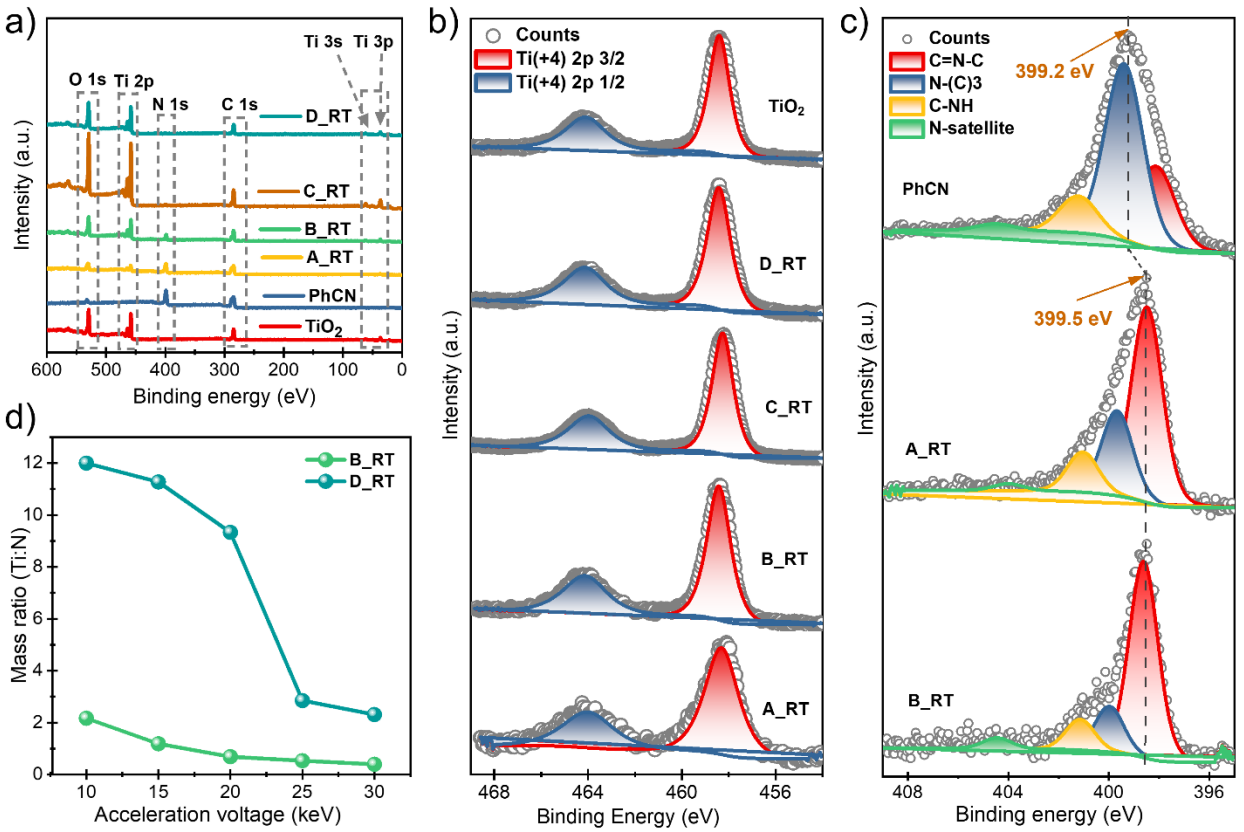

Figure 3. a) XPS survey spectra; b) XPS Ti2p spectra; c) XPS N1s spectra; d) Ti:N mass ratios in hybrids B_RT and D_RT with altering incident acceleration voltage calculated via EDS point mapping.

This implies that when titania grows onto the surface of PhCN, it may hamper the degree of polymerization in PhCN and thus hinder the integrity of the heptazine structure. The peak related to the N-$(C)_3$ bond of the hybrids shifts towards higher binding energy with higher TiO_2 content indicating a successful perturbation of the aromatic carbon nitride structure due to the presence of Ti which agrees with FTIR and TGA studies. On the other hand, the N1s spectra is very weak for C_RT and D_RT hybrids which is due to enhanced crystallization of TiO_2 on the surface *(Figure S9a, S9b)*.[23] The Ti 2p spectra (Figure 3b) of TiO_2 anatase shows peaks at 458.44 ($Ti2p_{3/2}$) and 464.14 eV ($Ti2p_{1/2}$) with a symmetric line shape and a spin orbit splitting of 5.7eV corresponding to the Ti^{4+} state. [36] The Ti2p spectra at 458.3eV is observable in all the as prepared hybrids

indicating the presence of TiO_2 on the surface (Figure 3b). The $Ti2p_{3/2}$ peak position in the hybrid A_RT shifts to a lower binding while it stays alike to pristine TiO_2 in hybrids B_RT and D_RT. This is due to the higher fraction of PhCN (i.e., N atoms) in the hybrid A_RT and comparatively much lower fraction of PhCN in the hybrids B_RT and D_RT. We could suggest that Ti sites on the surface of A_RT are well surrounded by a high number of electronegative N atoms causing the shift. When annealed at 400˚C, the nitrogen % in hybrid B drops to a lower value and the N1s spectrum becomes very weak *(Figure S10)* indicating loss of N related bonds due to annealing, at the same time Ti2p spectra of B_400 shows a shift of 0.1eV towards lower binding energy *(Figure S11)* due to the removal of electron rich N atoms from its vicinity. A higher count for Ti 2p signal is also observed, showing enhanced crystallization of TiO_2 in the annealed hybrid.[23]

Scanning electron microscopy (SEM) images show the evolution of the hybrid morphology occurring with increasing titania loadings *(Figure S12).* They show smaller particle size and agglomeration with increasing TiO_2 loading in the hybrids which is consistent which the SEM images of TiO_2 nanoparticles prepared with identical amounts of Ti precursor under identical solvothermal process *(Figure S13)*. When annealed, the hybrids do not show any considerable size changes through the SEM images *(Figure S14)* while for pristine TiO_2 nanoparticles, we observe an increase in the particle size *(Figure S13).* In addition, the SEM images of PhCN treated in the autoclave show larger distribution of particles with smaller diameters *(Figure S15),* which can enhance the surface area available for TiO_2 for nucleation. Next, we conducted detailed energy-dispersive X-ray spectroscopy (EDS) point analysis coupled with SEM with electron beam energies of 10keV, 15keV, 20keV, 25keV and 30keV, and observed the gradient of N from PhCN and Ti from TiO_2 in the hybrids. The hybrids B_RT and D_RT were penetrated by electrons with increasing acceleration voltages providing us the weight ratios of the constituent elements (Ti and N) at corresponding depths of the material (Figure 3d). The amount of Ti decreases with increasing depth in both samples, showing a gradient and confirming the major presence of TiO_2 on the PhCN surface as shown by XPS results. Meanwhile D_RT, in which the amount of Ti precursor was five-fold higher, shows higher percentage of Ti at greater depths of the sample. It must be noted that N was detected in both the hybrids at all acceleration voltage settings. This indicates a continuum of carbon nitride in-between the TiO_2 particles which ensures a strong connection between the two components – a structural characteristic favourable for charge transfer.[37]

Transmission electron microscopy (TEM) analysis was done to unravel the structural properties of the hybrids. The TEM images of TiO_2 nanoparticles show the presence of nano-crystallites, which further grow upon annealing at different temperatures *(Figure S16).* PhCN shows a typical g-C_3N_4 like structure with irregularly curved layers and tremella-like appearance (Figure 4a). [38] When autoclaving with low amounts of $TiCl_4$, the PhCN nanosheets become tightly overlapped with each other due to the high pressure (Figure 4b) and display minimal to no presence of TiO_2 crystallites. As the amount of Ti precursor is increased, we see the crystallization of TiO_2 around the PhCN nanostructures (Figure 4c, 4d) in the hybrid B_RT where we can observe intermeshed PhCN and TiO_2 on the surface where TiO_2 crystallites look like platelets on the background of PhCN. TEM images clearly show that the TiO_2 forms a layer around the irregular PhCN structures. B_RT exhibits a gradient core-shell morphology wherein the core of closely stacked PhCN nanosheets are decorated with small TiO_2 nano-crystallites all around the perimeter without large agglomeration (Figure 4c, 4d). It is possible to observe a continuous network of PhCN with TiO_2 in the hybrid B_RT. However, further increasing the TiO_2 loading results in inhomogeneous agglomeration spots of TiO_2 encapsulating PhCN as evident in sample C_RT and D_RT (Figure 4e, 4f). Additionally, we also observe breakage and random ordering of PhCN nanosheets in these samples. Furthermore, the effect of annealing the hybrids is identical to that as observed in TiO_2

nanoparticles *(Figure S17).* Hybrid A _400 shows TiO_2 nano-crystallites even when they were not observable in the as-prepared sample A_RT *(Figure S17a).* These observations show that the ratio of the precursors and the employment of thermal treatment plays an important role in the morphology of a hybrid system.

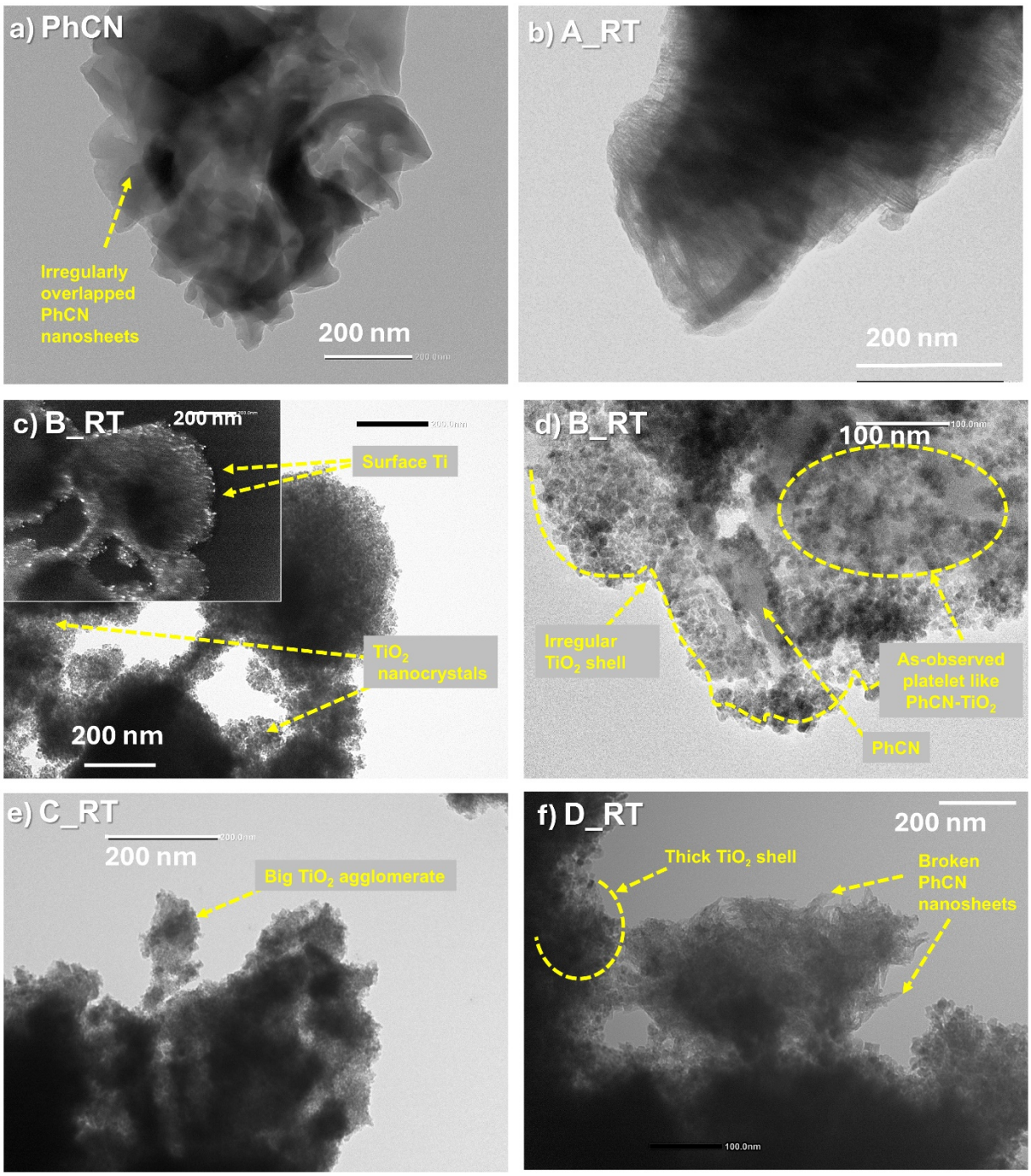

Figure 4. TEM images of a) Pristine Bulk PhCN, b) hybrid A_RT, c),d) hybrid B_RT with dark field image inset at c), e) hybrid C_RT and f) hybrid D_RT

The surface area of pristine TiO_2 nanoparticles shows a slight decrease with increased annealing temperatures (Table S3), accompanied by a reduction in micro- and mesopores, ultimately resulting in a predominantly macroporous material (Figure S18). In contrast, PhCN itself is non-porous, with a low surface area of 5.9 m^2/g (Figure S19). However, in the PhCN/TiO_2 hybrids, the porous TiO_2 outer shell contributes to significantly higher porosity (Table S4). Additionally, we observed that as the TiO_2 loading in the hybrids increases, so does the surface area, consistent with SEM images that reveal smaller particle sizes with higher TiO_2 content. When annealed, the hybrids exhibit a similar trend to pure TiO_2 nanoparticles, showing a decrease in surface area, as reflected in both BET analysis and SEM images (Table S5). This pattern likely results from the densification of the TiO_2 shell around the PhCN core during thermal treatment Through these results, it can be said that the structural evolution of PhCN/TiO_2 hybrids is synonymous to the structural evolution of TiO_2 nanocrystals present in them which is the fruit of TiO_2 crystallization on the surface of pristine PhCN during the solvothermal synthesis.

From the FTIR, TGA and XPS studies we can conclude the loss in the PhCN's heptazine integrity with increasing TiO_2 content in the hybrids. We thus propose that the nucleation of TiO_2 happens on the surface of stacked PhCN sheets and as the crystallization takes place during the solvothermal treatment; it cleaves some of the PhCN nanosheets on the surface of the matrix as shown in TEM (Figure 4f). With an increase in the dosage of Ti precursor, more PhCN sheets are cleaved without any formation of Ti-C or Ti-N bonds as corroborated by XPS C1s and N1s spectra and more TiO_2 crystallites are formed around the PhCN particles. The XPS, EDS and TEM studies show the presence of a PhCN core and a PhCN-TiO_2 layer around it in the hybrids. With higher $TiCl_4$ dosage, nucleation is prevented, and the TiO_2 growth is slowed down due to less availability of the free water content needed in the hydrolysis.[39] A similar trend is observed in the annealed hybrids. The extensive growth in the size of TiO_2 crystallites due to annealing leads to more rupture of PhCN nanosheets and the big crystallites form an outer shell shielding the PhCN core from the neighbouring environment. A schematic of this proposed structural evolution is given in Figure1.

3.2. Optical characterizations

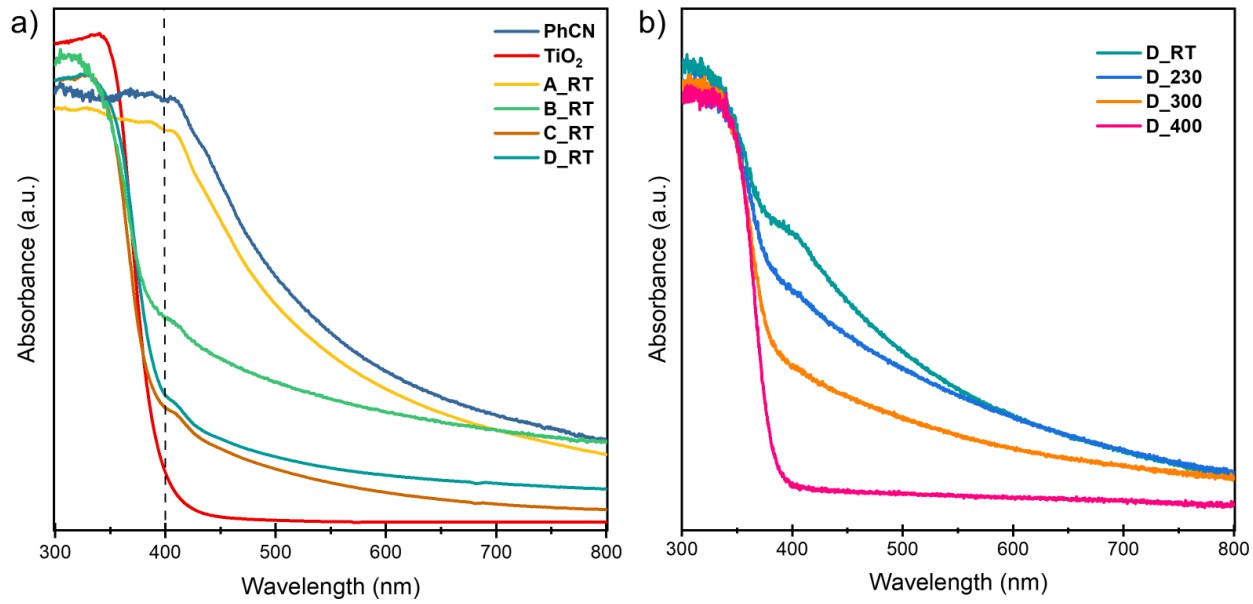

Figure 5 DRS absorption spectra of a) PhCN, TiO_2 and the as-prepared hybrids; b) hybrid D annealed at different temperatures.

The light-absorption behaviour of the solid hybrids was studied with diffuse-reflectance spectroscopy (DRS) to shed light on the interaction between the PhCN and TiO_2 semiconductors and the Kubelka-Munk transformation function was used to estimate the optical band gaps of the materials *(Figure S21-S25).* The reflection configuration measures the diffuse reflection of the sample with respect to a KBr reference that is considered to have 100% reflectivity. As shown in Figure 5a, TiO_2 absorbs from wavelengths lower than 400nm corresponding to a band gap of 3.2 eV, while PhCN shows considerable absorption in the visible range with a band gap of 2 eV. The autoclave-treatment of PhCN widens its bandgap to 2.3 eV and reduces the visible-light absorption *(Figure S20).* The as-prepared hybrids show light absorption extended throughout the visible range and a clearly visible absorption edge of TiO_2 at 390 nm (Figure 5a). The differential analysis of the absorption spectra of the as-prepared hybrids do not show any new optical band at energies lower than the energies of the absorption edge of either of the component indicating a case of a weak coupling, or the *photoinduced electron transfer*[17] where, the absorbed photons might result in the excitation of electron in the PhCN's HOMO to LUMO followed likely by a fast transfer to the conduction band of TiO_2. The absorption of the hybrids is controlled by the gradient core-shell structure, where a thick TiO_2 shell (in the case of C_RT and D_RT) shows low visible light absorption, a shell with equal distribution of PhCN and TiO_2 (B_RT) shows intermediate visible-light absorption and, low TiO_2 on the surface (A_RT) shows visible-light absorption identical to PhCN. When a hybrid is annealed, its visible light absorption decreases due to the removal of N atoms from the surface as confirmed by XPS *(Figure S10)*, resulting in the alteration of PhCN's chemical structure and hence, absorption properties.[7] This trend is most prominent in hybrids with highest TiO_2 content- hybrid D series (Figure 5b) where we can observe the sample annealed at higher temperature showing absorption spectra identical to TiO_2 due to a highly crystallized and thick outer TiO_2 shell and low availability of N atoms from the PhCN. The reduction in the surface

area and porosity of TiO_2 nanoparticles with annealing according to the BET data, also suggests a lower interaction of outer shell TiO_2 with PhCN and in turn less heterojunction formations which can also hamper the visible-light absorption. The optical bandgaps of the hybrid A series *(Figure S22-S25)* show no TiO_2 contribution in RT and 230^oC annealing but show the same when annealed at higher temperatures. The tauc plots of B,C and D series *(Figure S22-S25)* show similarities with TiO_2 band gap values as all of them contain titania in much higher ratios than hybrid A. A tentative increase in optical bandgap of the hybrids can be observed when TiO_2 amounts are increased.*(Figure S25)*

To study the excited state of the hybrid systems, we mapped the photoluminescence (PL) spectra of our samples with respect to excitation wavelength ranging from 300-600nm. The emission from bulk PhCN, consists of a broad emission between 450 and 650 nm peaked at 525 nm with a large excitation maximum between 350 and 420 nm (Figure 6a). This broad emission from PhCN is a function of generated excitonic species (bound e^- -h^+) and not separated e^- and h^+. The autoclave treatment of PhCN generates higher luminescence counts without any variation in the photoluminescence excitation range *(Figure S26).* It is observed that the profile of emission from PhCN does not change with the excitation wavelength, and it has the same PL profile under both UV and visible excitation (Figure 6a). This arises from the localization of excitons in the disordered regions of the material where the presence of phenyl groups introduces additional states that facilitate the trapping of excitons, leading to the formation of self-trapped excitons (STE).[40] The excitation-emission maps of the as-prepared hybrids (Figure 6b, 6c, 6d, 6e) show overall decrease in photoluminescence with increasing TiO_2 content. This quenching of PL indicates a reduced recombination of charge-carriers and a successful charge separation in the hybrids. The as-prepared samples also show a blue shift of the peak maximum (about 500 nm) and a restricted

range of the excitation spectrum between 360 and 420 nm due to the high absorption of the UV energy by the TiO_2 component in the hybrids as shown by the UV-Vis absorbance spectra. It must

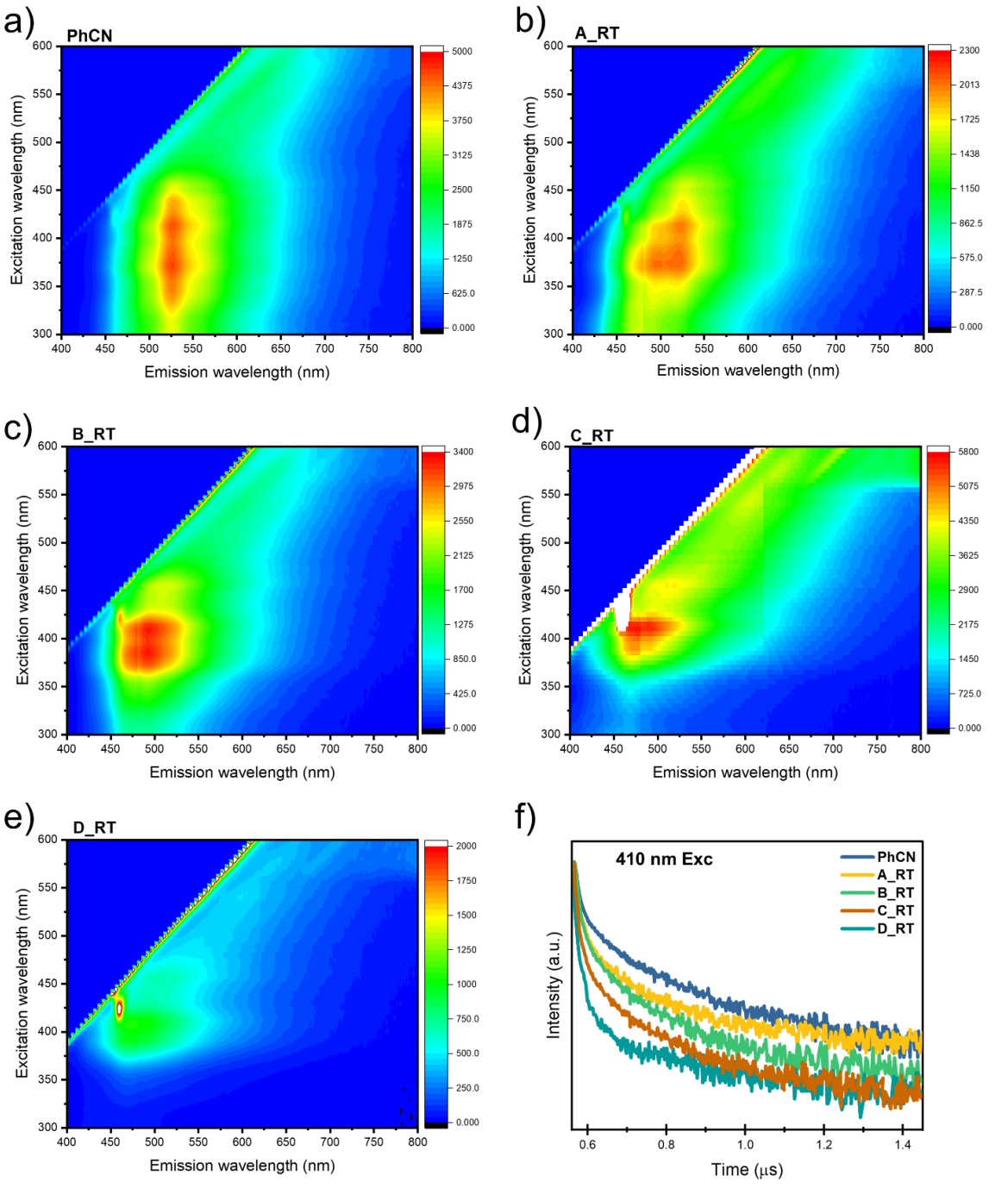

Figure 6 a), b), c), d), e) 3D steady-state luminescence maps of as-prepared PhCN, and hybrids A_RT,B_RT, C_RT, D_RT respectively with different maxima and minima values as indicated in the accompanying colour bar (the measurement for C_RT was done without a 10% filter at the excitation slit); f) Time-resolved photoluminescence measurement with an excitation wavelength 410nm and monitored emission wavelength from 440nm to 700nm..

be noted that only the emission from excitations below the wavelength 390 nm (the absorption edge of TiO_2) should have any absorption contribution from TiO_2. The PL spectra of B_RT also show a blue shift in the emission maxima which might be due to a higher contribution from the recombination from σ^* energy level of the PhCN[41]. The annealed hybrids show extremely low emission counts *(Figure S27)* and no excitation from the UV due to the presence of highly crystallized TiO_2.

The trapping of excitons on a timescale of picoseconds to nanoseconds, followed by slower relaxation processes in the microsecond region[40] can be studied by the time-resolved photoluminescence (TRPL) measurements. Generally, the time decay behaviour of excitons in PhCN can be well reproduced by three time-exponential curves with time decay of 35 ns, 150 ns and 750 ns.[12] The decay time profiles can be modelled using a multi-exponential decay function:

$$y = \sum_i A_i e^{-\frac{t}{\tau_i}} \quad (1)$$

The experimental time-resolved luminescence data relate to the recombination probability from the excited states through the equation:

$$\gamma_{tot} = \gamma_{rad} + \gamma_{NR} = \frac{1}{\tau_{rad}} + \frac{1}{\tau_{NR}} = \frac{1}{\tau_{tot}} \quad (2)$$

Here, i=1 or 2i=1 or 2 γ_{tot} represents the overall recombination probability from the excited state, with γ_{rad} and γ_{NR} being the probabilities for radiative and non-radiative recombination, respectively. τ_{rad} and τ_{NR} are the respective lifetimes of the radiative and non-radiative pathways, and τ_{tot}, the overall decay time, is determined experimentally through the fitting procedure. Hence the observed decrease in the recombination kinetics in the PL is due to the presence of the increased probability of non-radiative path. This effect can be well observed in Figure 6f, where a faster decay is observed from the σ* level of the PhCN. All the hybrid samples show a faster kinetics, related to the presence of new non-radiative channels (Figure 6f). The increased efficiency in the charge transfer mechanism in sample D_RT is due to the higher number of active organic sites. D_RT has most of the PhCN surface in close contact with titania generating the efficient charge transfer. The thermal treatment of the hybrids leads to low photoluminescence where annealing at 300˚C and above did not provide enough counts for a TRPL measurement *(Figure S28).* The optical characterization results show a successful charge-separation and charge transfer in the case of the as-prepared hybrids indicating that the hybrid structure has been achieved only by the solvothermal process without further annealing.

3.3. Photocatalytic Dye Degradation Tests

Rhodamine B (RhB)is an organic synthetic dye that is both harmful towards the ecosystem and extremely carcinogenic in nature causing various diseases in the human population. Therefore, it was selected as a model dye pollutant first, due to its high abundance and second, due to its excellent stability in industrial wastewater making its treatment difficult via other conventional

methods. The photocatalytic performances of the PhCN/TiO_2 hybrids were evaluated by monitoring their oxidative properties of RhB dye under visible light irradiation. To evaluate their photodegradation performance, dye concentration profiles were measured as a function of time under illumination using a commercial white LED with a sharp emission at 445 nm *(Supporting Information Section 1).* The tests were done in the presence of O_2 in ambient conditions. 2ml aliquots were taken every hour after illumination. 0.02mM concentration of dye was used for all degradation studies. Before illumination, the dye-photocatalyst system was kept in dark for 30 minutes to attain adsorption-desorption equilibrium. The effect of light on the dye was also studied without the presence of photocatalyst to look for any photodegradation.

Control experiments show no photo-degradation of RhB dye on visible light irradiation *(Figure S29),* and a small adsorption of the dye on the surfaces of the hybrids in the dark, indicating adsorption-desorption equilibrium. The photocatalytic degradation of RhB dye by PhCN and TiO_2 is shown by the Figure S30 a and b respectively. PhCN could degrade only 28.4% of the 0.02mM RhB solution in 7h while TiO_2 could degrdate only 7% of it. The photocatalytic tests with RhB and the PhCN/TiO_2 hybrids showed successful visible-light active photocatalytic degradation. (Figure 7a, 7b, 7c). The photodegradation performance was found to be in the order of A_RT < D_RT < C_RT < B_RT along with the pseudo-first-order rate constants of $0.6x10^{-2}$ min^{-1}, $2.3x10^{-2}$ min^{-1}, $1.4x10^{-2}$ min^{-1} and $0.80x10^{-2}$ min^{-1} respectively calculated by using Langmuir-Hinshelwood kinetic model. The photocatalytic performance of hybrid B degrades with annealing at higher temperatures and the as-prepared hybrid has the highest activity. For the photocatalysts annealed at 400˚C, hybrid B_400 showed the highest rate constant of $6.2 \times 10^{-3} min^{-1}$ followed by hybrids A_400, C_400 and D_400 which is the order of their increasing TiO_2 content.

The observed trends in the degradation of RhB can be related to the morphology of the hybrids revealed from TEM images (Figure 4.) where the less availability of TiO_2 on the surface can lead to worst photocatalytic performance for hybrid A, followed by an optimum level of interaction between PhCN and TiO_2 in hybrid B and an excess of TiO_2 agglomeration leading to a reduction in active catalytic surface for hybrids C and D.[10] When the hybrid B is annealed at different temperatures, the crystallinity of TiO_2 increases with the temperature alongside the band gap leading to lower RhB degradation. Through this detailed study, one could argue that the best performing photocatalyst is in its unannealed phase because of the superiority of solvothermal synthesis as a facile method to generate crystalline anatase hybrids with good crystallinity which has enough active sites to refrain further heat treatment.[19] The tendency of the moderate ratio of PhCN/TiO_2 (hybrid B) to outperform others indicates an optimised interaction between the PhCN core and the TiO_2 porous envelope suggesting the highest degree of charge extraction with lowest recombination rates. The observed substantial decrease in the photocatalytic ability of all the hybrids when annealed at 400˚C is likely related to the sintering of TiO_2 at higher temperatures and the corresponding loss of its active surface area along with the loss in the integrity of PhCN due to TiO_2 crystallization. In addition, when there is agglomeration of TiO_2 on the surface of PhCN core, it gets shielded from the incident light and cannot generate charged carriers. Recyclability tests were done for the best performing hybrid B_RT till 4 cycles of RhB degradation without observing any loss in the photocatalytic activity indicating its excellent stability *(Figure S31).* The test in the dark *(Figure S32)* shows that the removal of RhB by B_RT is solely due to photocatalysis without a major contribution from adsorption which enhances the reusability of the hybrid B_RT after a cycle of dye removal. All the above-mentioned discussion implies that we have successfully generated a hybrid which can be easily commercialised due to use of cheaper and readily available chemicals, ease of synthesis, reusability and practicality. Our hybrid is compared with some other advanced materials for the degradation of RhB in Table S6.

To investigate the main oxidation species responsible for the degradation of RhB dye, the identification of reactive oxygenated species (ROS) produced during the reaction is essential. For this, quenching tests were performed with 1mM solution of radical scavengers namely: NaN_3, IPA, $CHCl_3$, $AgNO_3$ and TEOA for the species O_2^{1}, OH^{*}, O_2^{*} , photogenerated e^{-}, and h^{+} respectively (Figure 7d). The tests were performed in identical conditions to that of the dye degradation tests.

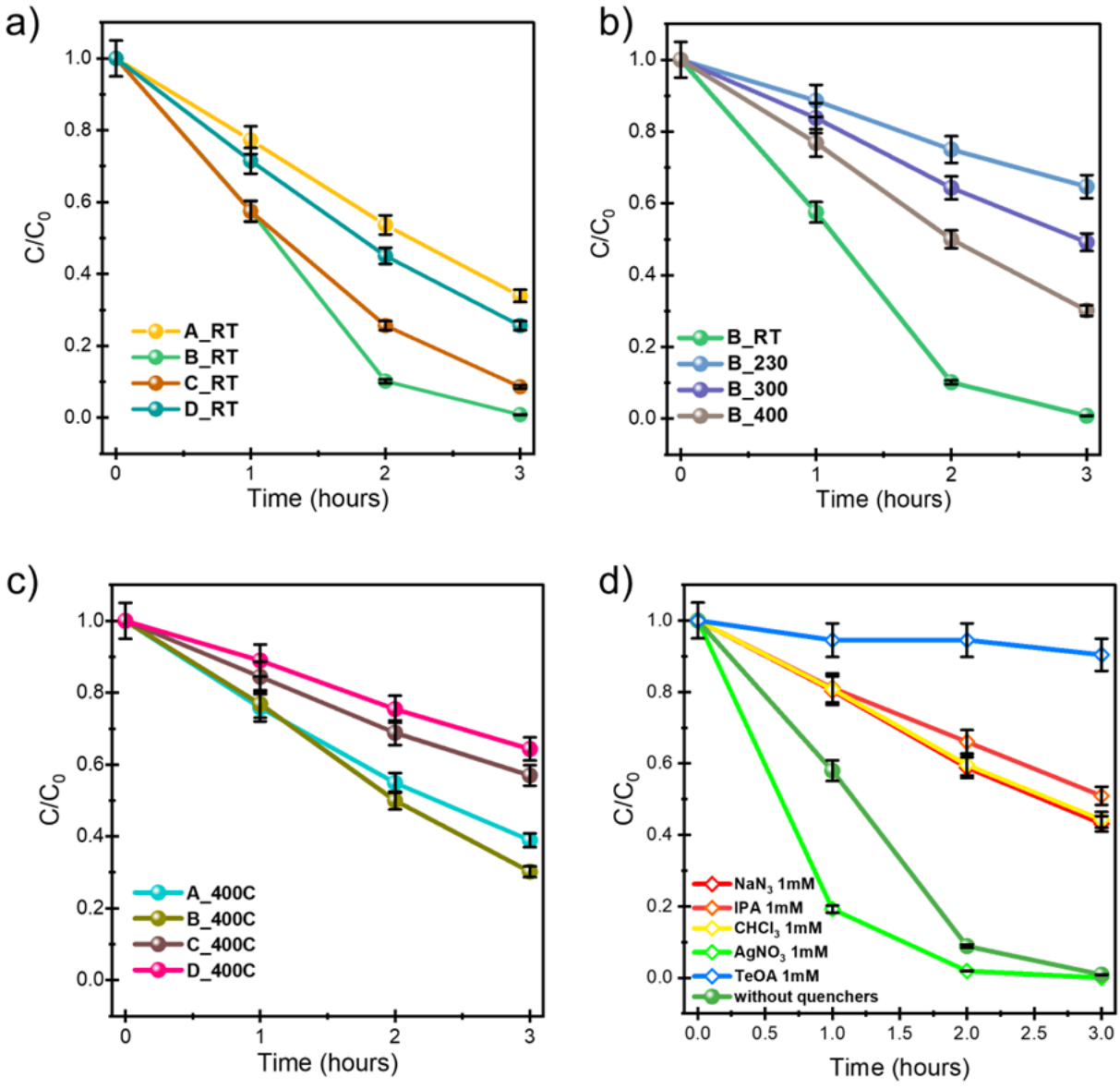

Figure 7 a),b),c) Photocatalytic degradation of rhodamine B dye by the PhCN/TiO_2 hybrids under visible light illumination. ;d) Quenching of the degradation of Rhodamine B by B_RT through radical scavengers.

It was observed that all the ROS were present during the intermediate reactions for RhB degradation. NaN_3 and $CHCl_3$ show identical quenching suggesting the origin of singlet oxygen and the superoxide radical from identical pathways. $AgNO_3$ accelerates the degradation of RhB, where Ag enhances the e^-h^+ separation process which was confirmed by the degradation of RhB dye by $AgNO_3$ in the absence of the photocatalyst *(Figure S33).* The quenching by IPA is higher than O^{2-} quencher and it acts as one of the major species for RhB degradation as evident by detailed quenching tests *(Figure S34)* where 50% v/v IPA shows complete stopage of the photocatalytic dye degradation. Amongst all, the use of TEOA hampers the photocatalytic degradation to the highest extent and stops the process completely when added at 100mM concentration *(Figure S35)*. This shows that the photogenerated holes were the predominant ROS responsible for the RhB degradation. The degradation of methylene blue (MB) and methyl orange (MO) dyes were also checked under visible-light illumination with hybrid B_RT as shown in figure S36a, S36b. It was observed that B_RT did not interact with MB either by photocatalytic degradation or adsorption, while MO was substantially adsorbed (60%) in 30mins by B_RT along with a red shift. Since MO is an anionic dye and MB is a cationic dye, the tests suggest that the surface of B_RT photocatalyst is positively supported by the abundance of holes. The red shift in the absorbance spectra of MO could be attributed to the polarity of the photocatalyst as MO is sensitive as a pH indicator. The pH of the reaction plays a significant role in influencing the photocatalytic degradation efficiency of the PhCN/TiO_2 hybrid. In general, pH adjustments can enhance or suppress the formation of reactive oxygen species (ROS), such as hydroxyl radicals, which are critical for the degradation of RhB.as shown by the quenching tests. The addition of a weak base like TEOA can raise the pH of an acidic environment but it resulted in complete quenching of RhB degradation in our case. Conversely, the addition of the hydroxyl radical quencher IPA lowers the pH, but it also inhibited photocatalytic RhB degradation, though to a lesser extent.

3.4. Photocatalytic H_2 production Tests

After evaluating the oxidative potential of our hybrids, we switched to the photocatalytic performance towards their sacrificial hydrogen evolution reaction (HER). Due to the higher dye degradation abilities of the as-prepared hybrids, only A_RT, B_RT, C_RT and D_RT were selected for the HER tests. The tests were conducted using a home-made closed reactor system with a constant temperature of 15˚C through water jacket cooling, 1wt% photo deposited Pt as the co-catalyst and 445nm LED illumination *(Supporting information, section 1)*. Hybrid B_RT was used to test two sacrificial agents, MeOH and TEOA, which are widely reported as an efficient sacrificial agent for TiO_2 and carbon nitrides, respectively.[42] We observed that B_RT produced 15 times more H_2 in the presence of 0.1M TEOA as compared to MeOH (Figure 8a), thereby suggesting that the holes are effectively scavenged from the PhCN part of the hybrid and not TiO_2. Therefore 0.1M TEOA was employed for the rest of the HER tests of all the as-prepared hybrids (Figure 8b). Like the RhB degradation tests, hybrid B_RT showed the highest HER activity among the as-prepared hybrids at an impressive 5789 μmol $h^{-1}g^{-1}$. Table S7 compares the H_2 production abilities of recently reported gCN based advanced photocatalysts. Compared to the case of the as-prepared PhCN *(Figure S37),* B_RT produces ~6.5 times more H_2 which can be ascribed to the successful formation of heterojunctions with TiO_2 enhancing charge separation as shown by the PL measurements. Since the holes are scavenged from the PhCN core, D_RT shows the lowest H_2 production due to shielding of the PhCN core by a thick TiO_2 outer cover and further leading to inaccessibility of holes to the electron donating TEOA. The HER results validate the superiority of the gradient core-shell structure of the PhCN/TiO_2 hybrid where loss of porosity and interaction with surrounding molecules lead to lower photocatalytic activity in the case of A_RT and C_RT.[43]

The HER ability of the best performing hybrid B_RT was further evaluated with the help of an in-flow online H_2 detection system over a period of 44 hours *(Experimental details in Supporting information, section 1; Figure S38).* The rate of hydrogen production was measured continuously for 44 hours instead of doing hourly injections. Figure 8d shows the first 24 hours of the test in 1st illumination cycle. The initial rate of hydrogen production was measured around 80 µmol h^{-1} during the first ~40 min of illumination using a 445nm LED. However, following this, the photocatalytic rate was found to decrease gradually to ~19.2 µmol h^{-1} over the course of 21 hours, which could be attributed to the agglomeration, growth, and potential leaching of the Pt nanoparticles on the surface of the hybrid, as observed by similar studies on TiO_2/Pt photosystems.[44]

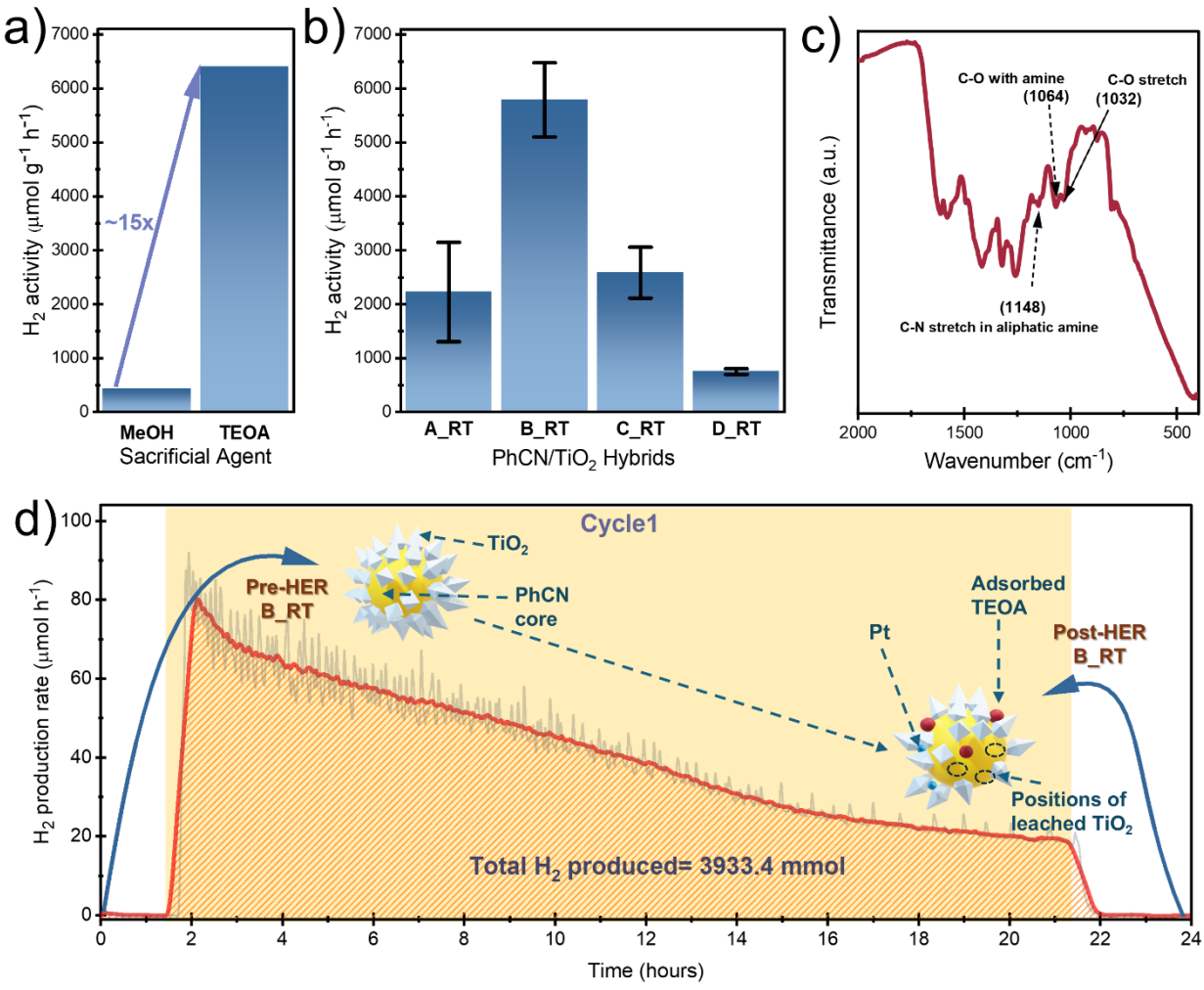

Figure 8 a) HER tests for sacrificial agent; b) HER tests of as-prepared hybrids; c) FTIR transmittance spectra of B_RT post flow HER test; d) Flow HER activity of B_RT for 1day.

To understand the process of deactivation of the hybrid, XRD, ATR-FTIR and XPS were performed on the hybrid B_RT post the flow HER reaction. XRD analysis showed all the characteristic reflections corresponding to PhCN and TiO_2 anatase, as observed in the pristine B_RT *(Figure*

S39). The IR absorbance of the photocatalyst after the flow tests showed the formation of aliphatic C-O and C-N bonds and enhancement of -OH and -NH stretches as compared to as-prepared B_RT (Figure 8c). These new absorbance peaks arise from the sacrificial agent used i.e., TEOA which is present in excess amounts (0.1 M) and may have adhered to the porous surface of our hybrid. Survey spectra obtained from XPS analysis *(Figure S40)* confirms the presence of C, O, N and Ti on the surface of the post-HER hybrid. A minor increase in the counts in the 70-72 eV region was observed suggesting the presence of small amount of Pt^0 on the surface.[44]

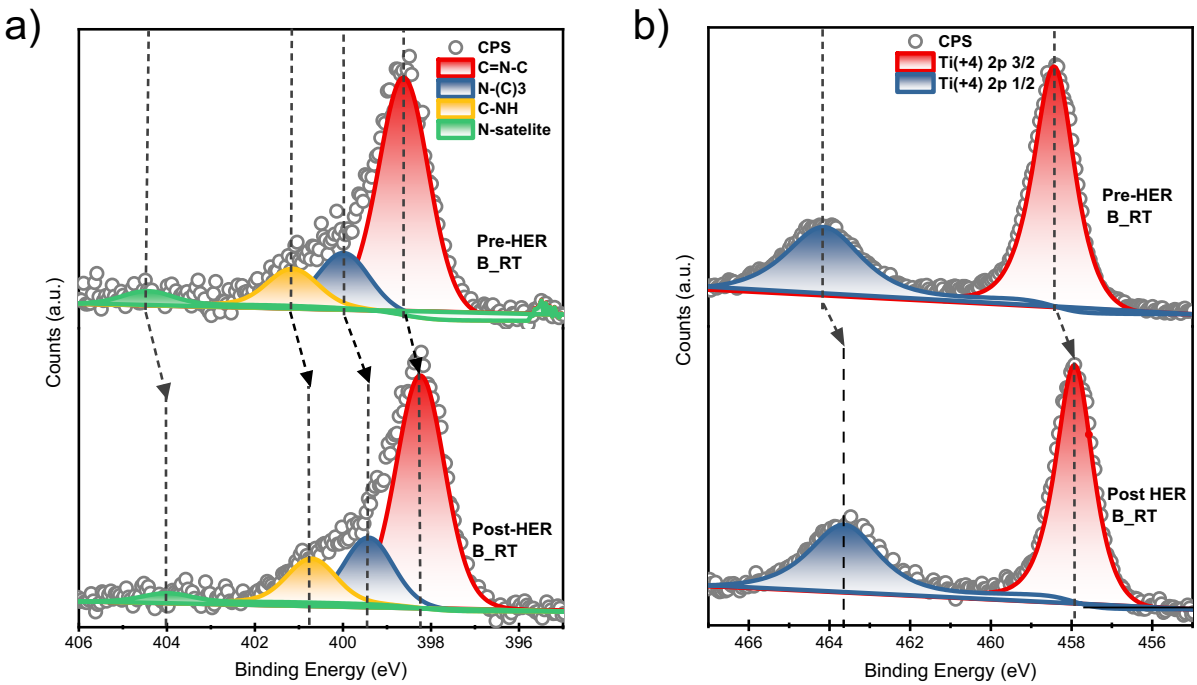

Figure 9 a),b) XPS N1s and Ti2p edges of B_RT post 2 day continuous HER test respectively.

However, due to the porous nature of the hybrid, it might be possible that some of the $PtCl_6^{2-}$ from the photo deposition process seeped into the pores of the hybrid at the PhCN/TiO_2 interface, which is not detectable by outer surface sensitive XPS.[44] The atomic concentration% quantification show an increase in the amount of N, a decrease in the amount of O and a substantial decrease in the Ti amounts from 10% to 4% in the post HER hybrid, which might suggest leaching of TiO_2 nanoparticles into the solution or a changing morphology of the hybrid. The N1s spectrum (Figure 9a) shows a shift of 0.3eV and Ti2p (Figure 9b) showed 0.5eV shift, both towards lower binding energy in the post HER B_RT. The O1s deconvoluted spectrum of the post-HER B_RT shows a major loss of Ti-O-Ti signal *(Figure S41).* All these observations indicate a partial reduction of the TiO_2 on the surface of the hybrid during the H_2 production.[45] Based on these results, we propose that this reduction of TiO_2 happens due to the surge of electrons flowing from PhCN to TiO_2. When illuminated using visible light, the photogenerated electrons from the PhCN goes towards the TiO_2 to increase the electron density around it causing the shift towards a lower binding energy. At the same time the lone pairs on N from the amine group of TEOA surrounds the PhCN resulting in the enhancement of electron density around N. While there have been a few reports studying such

behaviour[44–46], where the Ti-O bond is fractured during the photoreduction process creating oxygen vacancies and thereby recombination centres [46], it requires a reducing environment, and our experiments were carried out in a continuous gas flow system which deems this scenario to be highly unlikely.

3.5. Dual functional catalytic tests

Integrating pollutant degradation with hydrogen production in a single process can reduce operational costs compared to treating pollutants and producing hydrogen separately. Based on our structural and mechanistic insights, it was obvious that our hybrids are perfectly suited for simultaneous RhB degradation and HER where RhB molecules adsorbed on the surface of the hybrid would quench the holes and maintain a higher availability of electrons by photoexcitation for H_2 generation. At the same time, the dye molecules will also act as the source of protons necessary for a sustained HER. All experiments were performed using aqueous RhB dye solutions along with 1wt% Pt photodeposited onto B_RT without any additional sacrificial agents (Supporting information, section 1). Figure 10 shows that the hybrid B_RT is successfully able to produce H_2 while simultaneously oxidising RhB to CO_2 gas. We observe an initial rate of 8 µmol h^{-1} of H_2. Moreover, the H_2 production rate was further doubled when increasing the amount of RhB, with an optimal dye concentration of 0.04 mM for best HER results of 17.5 µmol h^{-1}, since further increasing the RhB concentration did not yield any improvement in the HER performance.

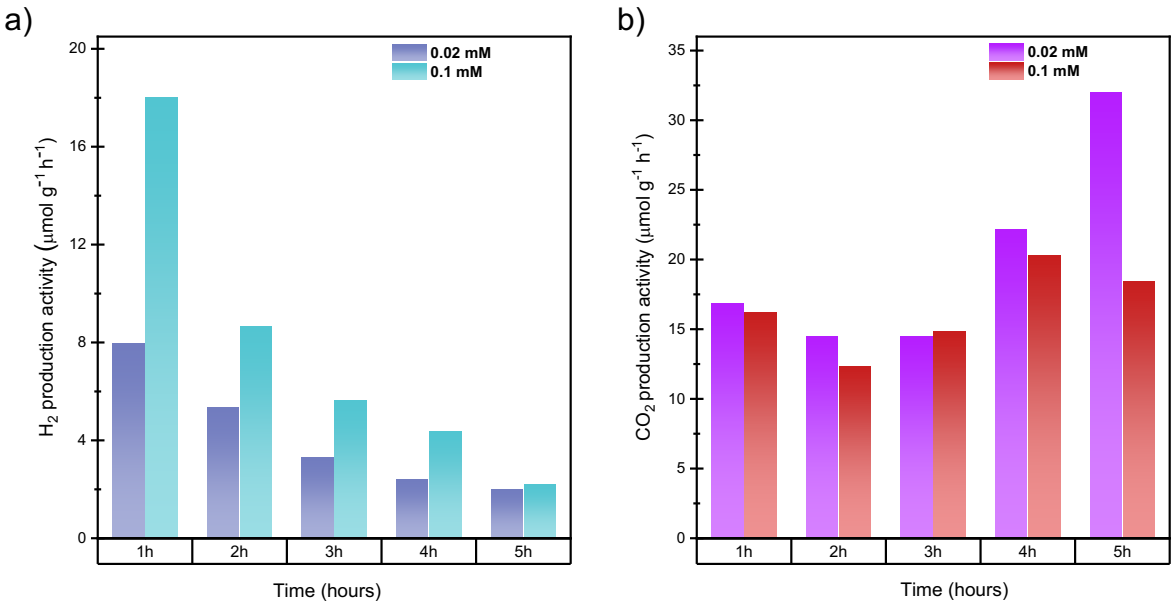

Figure 10 Simultaneous H_2 production a), and Rhodamine B dye degradation indicated by CO_2 evolution b) using PhCN/TiO_2 B_RT.

As expected, the amount of H_2 produced using RhB as the sacrificial agent was much lower than when with TEOA because of the high basicity of TEOA and its small molecular size which helps it to diffuse better in the pores of the hybrid photocatalyst leading to a more effective electron donation process.[2]Complementarily, the amount of evolved CO_2, as the product of RhB degradation, increased with time showing that more RhB molecules are being degraded (Figure

10b). However, longer illumination reveals a sharp decrease in the H_2 production rate which is first most likely due to the lack of sufficient amounts of RhB in the solution to consume the photogenerated holes, resulting in an increase in the number of charge-recombination, and secondly could be due to the agglomeration and deactivation of Pt NPs as suggested in section 2.5. Nonetheless, UV-Vis spectroscopic measurement confirmed the complete degradation of 0.02mM RhB after 5 h of illumination *(Figure S42),* along with a cease in any H_2 production further demonstrating that RhB acts as the source of CO_2 and H_2 (Figure 10a, 10b). Similar is the case with 0.1mM RhB *(Figure S43).* It is important to note that the negligible amount of H_2 produced in the latter half of the illumination cycle could also be due to the lack of dissolution of the dissolved H_2 in the reaction solution. Therefore, the successful production of H_2 by the degradation of RhB dye showed that the PhCN/TiO_2 hybrid B_RT has a good redox capability i.e., electron reduction through HER and hole oxidation through RhB degradation.

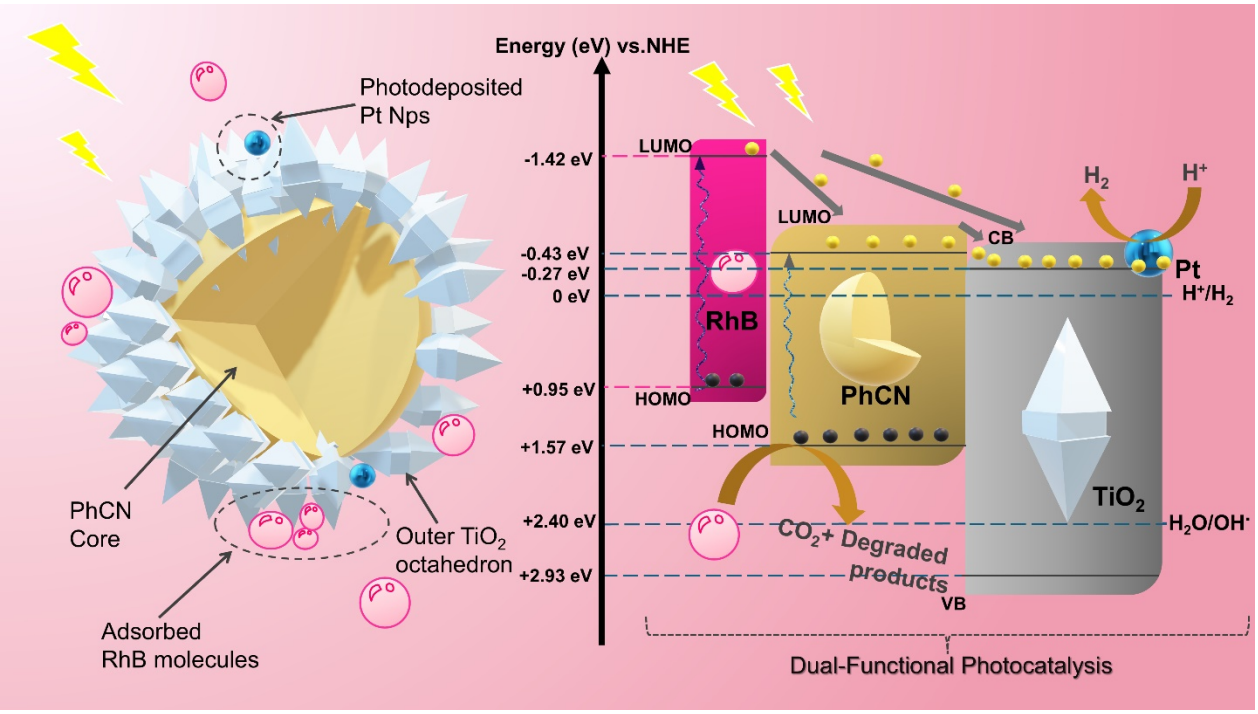

Figure 11. Type II charge transfer scheme of improved PhCN/TiO_2 hybrid for simultaneous Rhodamine B degradation and H_2 production under 445nm LED illumination.

Based on the results above, coupled with XPS analysis, optoelectronic studies and mechanistic insights, a mechanism of dual photocatalytic behaviour of oxidative coupling of RhB degradation integrated with H_2 evolution over PhCN/TiO_2 can be proposed as follows: 1)when the PhCN/TiO_2 hybrid comes in contact with the RhB molecules in water under dark conditions, it starts to adsorb the dye molecules onto its surface which is highly facilitated by the high porosity of the sample; 2) once the adsorption-desorption equilibrium is achieved in 30 mins and the visible light is incident to the system, the PhCN, owing to its suitable bandgap, absorbs visible-light photons and forms photogenerated e^- - h^+ pairs; 3) the adsorbed RhB molecules also get photoexcited owing to its LUMO and HOMO band positions at -1.42 and 0.95 eV (vs NHE) respectively[6] and Pt gets photodeposited on the surface of the hybrid via the reduction by the photoexcited electrons; 4)The photogenerated electrons from RhB migrate to the conduction band of TiO_2 as well as the LUMO of PhCN whereas the excited electrons from the LUMO band (σ* level) of PhCN are transferred to the conduction band of Ti due to the favourable alignment of their energy levels.[41] 5) the

deposited Pt acts as an electron acceptor due to the position of its fermi level which enhances the spatial charge separation and lowers the activation energy barrier to enhance the photocatalytic performance.[3] 6) the holes accumulated at the HOMO of PhCN react directly with the RhB molecules to further oxidize them to CO_2 and other degraded products; 8) Simultaneously the surface-adsorbed protons react with the localised trapped electrons on Pt to generate H_2 at the CB of TiO_2. This is a type II charge transfer mechanism where the photogenerated electrons and holes are utilised for H_2 production and oxidative degradation of Rhodamine B dye respectively, resulting in a dual-functional photocatalysis process. Figure 11 shows the dual-photocatalytic schematic representation of Type II charge-transfer pathway in the best PhCN/TiO_2 hybrid beside the E vs. NHE values of the components' band positions [41,47–49]. The reduction potential of H_2 is more positive than the conduction band potentials of both the components which allows the generation of H_2 via both. The presence of Pt and its indicative synergy with TiO_2 shows that TiO_2 is the principal generator in the HER. Since the oxidation potential of $OH^{\cdot}$ is more positive than the HOMO state of PhCN, $OH^{\cdot}$ are not generated via PhCN but TiO_2. The dye degradation happens majorly through the oxidation from the holes generated at the HOMO of PhCN. The irregular shape of the hybrid aids in the formation of maximum number of heterojunctions and the porous surface ensures a high interaction between the adsorbed species and the photogenerated charge carriers. The intermeshed structure guarantees less time for e^- h^+ recombination and shorter electron travel path from the PhCN core to the surface of the hybrid. Through this efficient pathway, the gradient core-shell PhCN/TiO_2 hybrid exhibits a good redox performance under visible light irradiation for dual-functional photocatalysis.

4. CONCLUSIONS

A highly efficient intermeshed gradient core-shell structure is reported via solvothermal approach with a core of visible-light active PhCN and a porous shell of crystalline PhCN-TiO_2 with impressive photocatalytic abilities. This work emphasizes on the importance of structural and morphological control of the hybrid photocatalytic system through detailed streamlining in the hybrid series. The nanoscale features have proven to be fundamental for the study of the photocatalytic efficiency. It was demonstrated that properties like surface area, porosity, and overall morphology of a system decides its photocatalytic activity and was found that the morphology of a system strongly influences the optoelectronic properties of a material, which can be controlled by utilising different synthetic procedures and thermal treatment. The gradient core-shell structure guarantees a high level of interaction between the semiconductor components of the hybrid as well as ensures a high interplay with surrounding molecules. Thermal treatment of the hybrids resulted in a decrease in the nitrogen content in the PhCN structure having a negative effect on the photocatalytic performance. Hence, the as-prepared hybrids always perform better. The crystallinity of the TiO_2 outer shell also aids in the photo-activity which can be ensured by a solvothermal synthesis. The optimised hybrid performs impressively as a visible-light active photocatalyst in the fast degradation of Rhodamine B dye via the formation of photogenerated holes as the major reactive species which can be coupled with simultaneous evolution of H_2 fuel. In this hybrid system, efficient and quick electron transfer from the LUMO state of the polymeric PhCN structure to the conduction band of TiO_2 plays an essential role. Both the σ^* and π^* excited states contribute to a non-radiative process, leading to a faster decay time. This suggests an electron transfer mechanism where the organic component (PhCN) acts as a sensitizer, transferring electrons to the TiO_2, which serves as the activator. A type II charge-transfer mechanism is proposed for the photocatalysis processes. Utilization of the industrial dye pollutant Rhodamine B for a clean H_2 fuel generation is a positive step towards achieving a circular economy. However, bio-friendly inorganic molecular co-catalysts need to be substituted for Pt to increase the lifetime of the catalyst and the H_2 production in the future. This comprehensive study and improvements can provide

prospects of continuing research in such a direction and act as a guide towards the design and study of new hybrid photocatalysts for dual functional photocatalysis.

Acknowledgments

The authors thank CeSAR (Centro Servizi Ricerca di Ateneo) core facility at the University of Cagliari for the ultrafast TR-PL, TEM, and XRD measurements. The authors gratefully acknowledge the Analytical Instrumentation Center (AIC) at TU Wien under the guidance of Dr. Annette Foelske for facilitating XPS measurements. MH acknowledges the Royal Society of Chemistry for the Researcher Development and Travel Grant (D23-2324506310) and the ERADOC Erasmus+ fellowship for funding the mobility between the two Universities. HR and SNM acknowledge the support by the Austrian Science Fund (FWF) doctoral college TU-Dx (DOC 142-N) as well as projects P32801-N and Cluster of Excellence MECS (10.55776/COE5).

Supporting Information

The supporting information is available free of charge at

- Elucidation of Core-shell Structure in Phenyl Grafted Carbon Nitride/TiO2 Nanohybrids for Visible-light Mediated H2 Production with Simultaneous Rhodamine B Degradation. (PDF)
- Materials and methods (S-3 - S-6), XRD (S-7 – S-8), FTIR and Raman data (S-9 – S-11), TGA and XPS (S-12 – S-15), Microscopy (S-16 – S-19), Surface area and porosity (S-20 – S-21), Optical Characterization (S-22 – S-28), Photocatalytic evaluation (S-29 – S-38), references (S-39 – S-40)

CRediT authorship contribution statement

Moulika Hazra: Conceptualization, Methodology, Formal analysis, Investigation, Project administration, Writing – original draft. **Stefania Porcu:** Methodology, Investigation, Formal analysis, Validation, Project administration, Writing – review and editing. **Stephen N. Myakala:** Investigation, Formal analysis, Visualization, Writing – review and editing. **Hannah Rabl:** Formal analysis, Investigation, Writing – review and editing**. Dominik Eder:** Resources, Supervision, Validation. **Alexey Cherevan:** Conceptualization, Formal analysis, Methodology, Supervision, Writing – review and editing**. Pier C. Ricci:** Conceptualization, Formal analysis, Funding acquisition, Resources, Supervision, Visualization, Writing – review and editing.

Funding statement

This work has been developed within the framework of the project e.INS- Ecosystem of Innovation for Next Generation Sardinia (cod. ECS 00000038) funded by the Italian Ministry for Research and Education (MUR) under the National Recovery and Resilience Plan (NRRP) - MISSION 4 COMPONENT 2, "From research to business" INVESTMENT 1.5, "Creation and strengthening of Ecosystems of innovation" and construction of "Territorial R and D Leaders".

Data availability statement

All relevant data are within the manuscript and its additional files.

Declaration of Competing Interest

This work has not been published previously and is not under consideration for publication elsewhere. It is approved by all authors and host authorities. No author has financial or other contractual agreements that might cause any conflict of interest.

References

(1) UNESCO World Water Assessment Programme. *The United Nations World Water Development Report 2024: Water for Prosperity and Peace*; 2024.

(2) Kampouri, S.; Nguyen, T. N.; Spodaryk, M.; Palgrave, R. G.; Züttel, A.; Smit, B.; Stylianou, K. C. Concurrent Photocatalytic Hydrogen Generation and Dye Degradation Using MIL-125-NH2 under Visible Light Irradiation. *Adv Funct Mater* **2018**, *28* (52). https://doi.org/10.1002/adfm.201806368.

(3) Wang, L.; Zhao, Y.; Zhang, B.; Wu, G.; Wu, J.; Hou, H. Spatial Separation of Redox Centers for Boosting Cooperative Photocatalytic Hydrogen Evolution with Oxidation Coupling of Benzylamine over Pt@UiO-66-NH2@ZnIn2S4. *Catal Sci Technol* **2023**, *13* (8), 2517–2528. https://doi.org/10.1039/d3cy00089c.

(4) Porcu, S.; Secci, F.; Ricci, P. C. Advances in Hybrid Composites for Photocatalytic Applications: A Review. *Molecules*. MDPI October 1, 2022. https://doi.org/10.3390/molecules27206828.

(5) Yan, T.; Yang, Q.; Feng, R.; Ren, X.; Zhao, Y.; Sun, M.; Yan, L.; Wei, Q. Highly Effective Visible-Photocatalytic Hydrogen Evolution and Simultaneous Organic Pollutant Degradation over an Urchin-like Oxygen-Doped MoS2/ZnIn2S4 Composite. *Front Environ Sci Eng* **2022**, *16* (10). https://doi.org/10.1007/s11783-022-1566-z.

(6) Xia, G.; Xiao, S.; Su, J.; Zhou, H.; Liu, Y.; Zhu, X. A Dual-Functional Catalyst: Wood-Templated BiVO4-CdS for Wood Dye Wastewater. *RSC Adv* **2023**, *13* (3), 1823–1833. https://doi.org/10.1039/d2ra06735h.

(7) Musa, E. N.; Kaur, S.; Gallagher, T. C.; Anthony, T. M.; Stickle, W. F.; Árnadóttir, L.; Stylianou, K. C. Two Birds, One Stone: Coupling Hydrogen Production with Herbicide Degradation over Metal-Organic Framework-Derived Titanium Dioxide. *ACS Catal* **2023**, *13* (6), 3710–3722. https://doi.org/10.1021/acscatal.3c00265.

(8) Huong, V. H.; Loan, T. T.; Pham, K. P.; Ha, M. N.; Nguyen, Q. H.; Ma, Y. R.; Ngac, A. B.; Nguyen, V. C. Unveiling the Synergistic Interplay of Appropriate Oxygen Vacancies and S-Scheme Heterojunction Structures in OVs-TiO2/g-C3N4 Catalyst for Efficient RhB Photodegradation and H2 Production. *J Alloys Compd* **2024**, *972*. https://doi.org/10.1016/j.jallcom.2023.172722.

(9) Li, B.; Zhang, B.; Zhang, Y.; Zhang, M.; Huang, W.; Yu, C.; Sun, J.; Feng, J.; Dong, S.; Sun, J. Porous G-C3N4/TiO2 S-Scheme Heterojunction Photocatalyst for Visible-Light Driven H2-Production and Simultaneous Wastewater Purification. *Int J Hydrogen Energy* **2021**, *46* (64), 32413–32424. https://doi.org/10.1016/j.ijhydene.2021.07.090.

(10) Dehkordi, A. B.; Badiei, A. Insight into the Activity of TiO2@nitrogen-Doped Hollow Carbon Spheres Supported on g-C3N4 for Robust Photocatalytic Performance. *Chemosphere* **2022**, *288*. https://doi.org/10.1016/j.chemosphere.2021.132392.

(11) Yan, L.; Zhong, S.; Xiao, C.; Chen, Y. Optimization of Hydrothermal Pretreatment to Prepare G-C3N4 with Enhanced Catalyst Yield and Photocatalytic Activity for Aqueous Contaminant Removal. *Materials Today Sustainability* **2023**, *22*. https://doi.org/10.1016/j.mtsust.2023.100374.

(12) Porcu, S.; Roppolo, I.; Salaun, M.; Sarais, G.; Barbarossa, S.; Casula, M. F.; Carbonaro, C. M.; Ricci, P. C. Come to Light: Detailed Analysis of Thermally Treated Phenyl Modified Carbon Nitride Polymorphs for Bright Phosphors in Lighting Applications. *Appl Surf Sci* **2020**, *504*. https://doi.org/10.1016/j.apsusc.2019.144330.

(13) Akhundi, A.; Zaker Moshfegh, A.; Habibi-Yangjeh, A.; Sillanpää, M. Simultaneous Dual-Functional Photocatalysis by g-C3N4-Based Nanostructures. *ACS ES and T Engineering*. American Chemical Society April 8, 2022, pp 564–585. https://doi.org/10.1021/acsestengg.1c00346.

(14) Dong, M.; Yu, J.; Wang, J.; Zhang, Q.; Lin, W. Construction of Phenyl-Grafted Carbon Nitride for Enhancing the Visible-Light Activity. *Chem Phys Lett* **2019**, *737*. https://doi.org/10.1016/j.cplett.2019.136817.

(15) Warshagha, M. Z. A.; Muneer, M. Synthesis of Ph-Modified Graphitic Carbon Nitride for Degradation of Different Chromophoric Organic Pollutants in Aqueous Suspension under Visible Light. *Langmuir* **2020**, *36* (33), 9719–9727. https://doi.org/10.1021/acs.langmuir.0c01055.

(16) Dai, A.; Huang, Z.; Tian, L.; Zhang, Z.; Guan, X.; Guo, L. Phenyl-Incorporated Carbon Nitride Photocatalyst with Extended Visible-Light-Absorption for Enhanced Hydrogen Production from Water Splitting. *J Colloid Interface Sci* **2022**, *622*, 494–502. https://doi.org/10.1016/j.jcis.2022.04.159.

(17) Wei, H.; McMaster, W. A.; Tan, J. Z. Y.; Cao, L.; Chen, D.; Caruso, R. A. Mesoporous TiO2/g-C3N4 Microspheres with Enhanced Visible-Light Photocatalytic Activity. *Journal of Physical Chemistry C* **2017**, *121* (40), 22114–22122. https://doi.org/10.1021/acs.jpcc.7b06493.

(18) Zhang, G.; Zhang, T.; Li, B.; Jiang, S.; Zhang, X.; Hai, L.; Chen, X.; Wu, W. An Ingenious Strategy of Preparing TiO 2 /g-C 3 N 4 Heterojunction Photocatalyst: In Situ Growth of TiO 2 Nanocrystals on g-C 3 N 4 Nanosheets via Impregnation-Calcination Method. *Appl Surf Sci* **2018**, *433*, 963–974. https://doi.org/10.1016/j.apsusc.2017.10.135.

(19) Wang, W.; Fang, J.; Shao, S.; Lai, M.; Lu, C. Compact and Uniform TiO2@g-C3N4 Core-Shell Quantum Heterojunction for Photocatalytic Degradation of Tetracycline Antibiotics. *Appl Catal B* **2017**, *217*, 57–64. https://doi.org/10.1016/j.apcatb.2017.05.037.

(20) Wang, J.; Yang, Z.; Gao, X.; Yao, W.; Wei, W.; Chen, X.; Zong, R.; Zhu, Y. Core-Shell g-C3N4@ZnO Composites as Photoanodes with Double Synergistic Effects for Enhanced Visible-Light Photoelectrocatalytic Activities. *Appl Catal B* **2017**, *217*, 169–180. https://doi.org/10.1016/j.apcatb.2017.05.034.

(21) Wassner, M.; Eckardt, M.; Gebauer, C.; Hüsing, N.; Behm, R. J. Spherical Core–Shell Titanium (Oxy)Nitride@Nitrided Carbon Composites as Catalysts for the Oxygen Reduction Reaction: Synthesis and Electrocatalytic Performance. *ChemElectroChem* **2016**, *3* (10), 1641–1654. https://doi.org/10.1002/celc.201600246.

(22) Porcu, S.; Maloccu, S.; Corona, A.; Hazra, M.; David, T. C.; Chiriu, D.; Carbonaro, C. M.; Tramontano, E.; Ricci, P. C. Visible Light-Mediated Inactivation of H1N1 Virus UsingPolymer-Based Heterojunction Photocatalyst. *Polymers (Basel)* **2023**, *15* (11). https://doi.org/10.3390/polym15112536.

(23) Mohamed, M. A.; Jaafar, J.; M. Zain, M. F.; Minggu, L. J.; Kassim, M. B.; Rosmi, M. S.; Alias, N. H.; Mohamad Nor, N. A.; W. Salleh, W. N.; Othman, M. H. D. In-Depth Understanding of Core-Shell Nanoarchitecture Evolution of g-C 3 N 4 @C, N Co-Doped Anatase/Rutile: Efficient Charge Separation and Enhanced Visible-Light Photocatalytic Performance. *Appl Surf Sci* **2018**, *436*, 302–318. https://doi.org/10.1016/j.apsusc.2017.11.229.

(24) Ma, R.; He, Y.; Feng, J.; Hu, Z. Y.; Van Tendeloo, G.; Li, D. A Facile Synthesis of Ag@PdAg Core-Shell Architecture for Efficient Purification of Ethene Feedstock. *J Catal* **2019**, *369*, 440–449. https://doi.org/10.1016/j.jcat.2018.11.037.

(25) Singh, A. P.; Arora, P.; Basu, S.; Mehta, B. R. Graphitic Carbon Nitride Based Hydrogen Treated Disordered Titanium Dioxide Core-Shell Nanocatalyst for Enhanced Photocatalytic and Photoelectrochemical Performance. *Int J Hydrogen Energy* **2016**, *41* (13), 5617–5628. https://doi.org/10.1016/j.ijhydene.2016.02.029.

(26) Wang, Y.; Yang, W.; Chen, X.; Wang, J.; Zhu, Y. Photocatalytic Activity Enhancement of Core-Shell Structure g-C3N4@TiO2 via Controlled Ultrathin g-C3N4 Layer. *Appl Catal B* **2018**, *220*, 337–347. https://doi.org/10.1016/j.apcatb.2017.08.004.

(27) Carneiro, J. T.; Savenije, T. J.; Moulijn, J. A.; Mul, G. How Phase Composition Influences Optoelectronic and Photocatalytic Properties of TiO2. *Journal of Physical Chemistry C* **2011**, *115* (5), 2211–2217. https://doi.org/10.1021/jp110190a.

(28) Singh, P.; Singh, S.; Maddiboyina, B.; Kandalam, S.; Walski, T.; Bohara, R. A. Hybrid Silver Nanoparticles: Modes of Synthesis and Various Biomedical Applications. *Electron* **2024**, *2* (2). https://doi.org/10.1002/elt2.22.

(29) Visser, N. L.; Daoura, O.; Plessow, P. N.; Smulders, L. C. J.; de Rijk, J. W.; Stewart, J. A.; Vandegehuchte, B. D.; Studt, F.; van der Hoeven, J. E. S.; de Jongh, P. E. Particle Size Effects of Carbon Supported Nickel Nanoparticles for High Pressure CO2 Methanation. *ChemCatChem* **2022**, *14* (22). https://doi.org/10.1002/cctc.202200665.

(30) Yan, P.; Zhang, Y.; Zheng, S. Microscale Spherical TiO2 Powder Prepared by Hydrolysis of TiCl4 Solution: Synthesis and Kinetics. *Particuology* **2024**, *84*, 60–71. https://doi.org/10.1016/j.partic.2023.03.004.

(31) Brinker, C. J.; Scherer, G. W. Sol --> Gel --> Glass: Gelation and Gel Structure. *J Non Cryst Solids* **1985**, *70*, 301–322. https://doi.org/https://doi.org/10.1016/0022-3093(85)90103-6.

(32) Zhang, J.; Sun, P.; Jiang, P.; Guo, Z.; Liu, W.; Lu, Q.; Cao, W. The Formation Mechanism of TiO2 Polymorphs under Hydrothermal Conditions Based on the Structural Evolution of [Ti(OH)h(H2O)6-h]4-h Monomers. *J Mater Chem C Mater* **2019**, *7* (19), 5764–5771. https://doi.org/10.1039/c9tc00662a.

(33) Li, G.; Li, L.; Boerio-Goates, J.; Woodfield, B. F. High Purity Anatase TiO2 Nanocrystals: Near Room-Temperature Syntheis, Grain Growth Kinetics, and Surface Hydration Chemistry. *JACS Articles* **2005**, *127* (24), 8659–8666. https://doi.org/10.1021/ja050517g.

(34) Roškaric, M.; Žerjav, G.; Zavašnik, J.; Pintar, A. The Influence of Synthesis Conditions on the Visible-Light Triggered Photocatalytic Activity of g-C3N4/TiO2composites Used in AOPs. *J Environ Chem Eng* **2022**, *10* (3). https://doi.org/10.1016/j.jece.2022.107656.

(35) Wang, Y.; Yu, J.; Peng, W.; Tian, J.; Yang, C. Novel Multilayer TiO2 Heterojunction Decorated by Low G-C3N4 Content and Its Enhanced Photocatalytic Activity under UV, Visible and Solar Light Irradiation. *Sci Rep* **2019**, *9* (1). https://doi.org/10.1038/s41598-019-42438-w.

(36) Liu, C.; Niu, H.; Wang, D.; Gao, C.; Said, A.; Liu, Y.; Wang, G.; Tung, C. H.; Wang, Y. S-Scheme Bi-Oxide/Ti-Oxide Molecular Hybrid for Photocatalytic Cycloaddition of Carbon Dioxide to Epoxides. *ACS Catal* **2022**, *12* (14), 8202–8213. https://doi.org/10.1021/acscatal.2c02256.

(37) Le, T. L. T.; Le, T. H. T.; Nguyen Van, K.; Van Bui, H.; Le, T. G.; Vo, V. Controlled Growth of TiO2 Nanoparticles on Graphene by Hydrothermal Method for Visible-Light Photocatalysis. *Journal of Science: Advanced Materials and Devices* **2021**, *6* (4), 516–527. https://doi.org/10.1016/j.jsamd.2021.07.003.

(38) Zhao, Z.; Sun, Y.; Luo, Q.; Dong, F.; Li, H.; Ho, W. K. Mass-Controlled Direct Synthesis of Graphene-like Carbon Nitride Nanosheets with Exceptional High Visible Light Activity. Less Is Better. *Sci Rep* **2015**, *5*. https://doi.org/10.1038/srep14643.

(39) Yang, Y.; Wang, S.; Ji, W.; Li, T.; Li, S.; Zhao, Q.; Li, G. TiCl4 Precursor Affecting the Performance of HTM-Free Carbon-Based Perovskite Solar Cell. *Nanotechnology* **2024**, *35* (7). https://doi.org/10.1088/1361-6528/ad0d22.

(40) Yu, J.; Wang, Y.; Zhou, Y.; Fang, W.; Liu, B.; Xing, J. Intrinsic Self-Trapped Excitons in Graphitic Carbon Nitride. *Nano Lett* **2024**, *24* (15), 4439–4446. https://doi.org/10.1021/acs.nanolett.4c00238.

(41) Porcu, S.; Castellino, M.; Roppolo, I.; Carbonaro, C. M.; Palmas, S.; Mais, L.; Casula, M. F.; Neretina, S.; Hughes, R. A.; Secci, F.; Ricci, P. C. Highly Efficient Visible Light Phenyl Modified Carbon Nitride/TiO2 Photocatalyst for Environmental Applications. *Appl Surf Sci* **2020**, *531*. https://doi.org/10.1016/j.apsusc.2020.147394.

(42) Kumaravel, V.; Imam, M. D.; Badreldin, A.; Chava, R. K.; Do, J. Y.; Kang, M.; Abdel-Wahab, A. Photocatalytic Hydrogen Production: Role of Sacrificial Reagents on the Activity of Oxide, Carbon, and Sulfide Catalysts. *Catalysts* **2019**, *9* (3). https://doi.org/10.3390/catal9030276.

(43) Dai, D.; Qiu, J.; Xia, G.; Tang, Y.; Yao, J. Defect Engineering Promoted Photocatalysis for Lignin Depolymerization: Performance and Mechanism Insight. *ACS Catal* **2023**, *13* (22), 14987–14995. https://doi.org/10.1021/acscatal.3c03462.

(44) Haselmann, G. M.; Eder, D. Early-Stage Deactivation of Platinum-Loaded TiO2 Using in Situ Photodeposition during Photocatalytic Hydrogen Evolution. *ACS Catal* **2017**, *7* (7), 4668–4675. https://doi.org/10.1021/acscatal.7b00845.

(45) Zhang, J.; Toe, C. Y.; Kumar, P.; Scott, J.; Amal, R. Engineering Defects in TiO2 for the Simultaneous Production of Hydrogen and Organic Products. *Appl Catal B* **2023**, *333*. https://doi.org/10.1016/j.apcatb.2023.122765.

(46) Shu, Z.; Cai, Y.; Ji, J.; Tang, C.; Yu, S.; Zou, W.; Dong, L. Pt Deposites on Tio2 for Photocatalytic H2 Evolution: Pt Is Not Only the Cocatalyst, but Also the Defect Repair Agent. *Catalysts* **2020**, *10* (9), 1–12. https://doi.org/10.3390/catal10091047.

(47) Tan, Y.; Shu, R.; Xu, H.; Song, L.; Zhang, R.; Ouyang, C.; Xia, M.; Hou, J.; Zhang, X.; Yuan, Y.; Zhang, R. Supercritical Carbon Dioxide-Assisted TiO2/g-C3N4 Heterostructures Tuning for Efficient Interfacial Charge Transfer and Formaldehyde Photo-Degradation. *J Environ Chem Eng* **2023**, *11* (5). https://doi.org/10.1016/j.jece.2023.110992.

(48) Acharya, R.; Parida, K. A Review on TiO2/g-C3N4 Visible-Light-Responsive Photocatalysts for Sustainable Energy Generation and Environmental Remediation. *Journal of Environmental Chemical Engineering*. Elsevier Ltd August 1, 2020. https://doi.org/10.1016/j.jece.2020.103896.

(49) Bledowski, M.; Wang, L.; Ramakrishnan, A.; Khavryuchenko, O. V.; Khavryuchenko, V. D.; Ricci, P. C.; Strunk, J.; Cremer, T.; Kolbeck, C.; Beranek, R. Visible-Light Photocurrent Response of TiO2-Polyheptazine Hybrids: Evidence for Interfacial Charge-Transfer Absorption. *Physical Chemistry Chemical Physics* **2011**, *13* (48), 21511–21519. https://doi.org/10.1039/c1cp22861g.

Table of contents Only